Waikato Regional Council Technical Report 2026/07

Catchment-scale LiDAR-based SedNetNZ modelling in the Upper Waitomo catchment

ISSN 2230-4347 (Online)
waikatoregion.govt.nz

Prepared by	Simon Vale, Hugh Smith, & Maksym Polyakov (Bioeconomy Science Institute Maiangi Taiao)
For	Waikato Regional Council Private Bag 3038 Waikato Mail Centre HAMILTON 3240
Publication date	August 2026
Document ID	35878983

	Name	Date
Peer Reviewer	Annette Semadeni-Davies	August 2026
Approving Manager	Michelle Begbie	August 2026

Catchment-scale LiDAR-based SedNetNZ modelling in the Upper Waitomo catchment

March 2026

Simon Vale, Hugh Smith, Maksym Polyakov

Bioeconomy Science Institute Maiangi Taiao

Contract Report registration number: 2526-0100

Prepared for: Waikato Regional Council

Reviewed by:
Andrew Neverman
Senior Researcher - Geomorphology / Erosion and Sediment Processes and Research Priority Area Leader
Bioeconomy Science Institute

Approved for release by:
Sam Carrick
Group Portfolio Leader – Land Resources & Climate Change
Bioeconomy Science Institute

Contents

Summary

Project and client

- Waikato Regional Council (WRC) contracted the Bioeconomy Science Institute Maiangi Taiao (BSI)[1] to model erosion and suspended sediment loads using the LiDAR-based version of the SedNetNZ model in the upper Waitomo catchment (44 km^2) to support integrated catchment management (ICM).
- The project involved generating a new digital stream network (DSN) from a 5 m digital elevation model (DEM) of the catchment that incudes modifications to represent sinkholes and subterranean conduits characteristic of the dominant karst landscape in the Waitomo catchment. A high-resolution landslide susceptibility model was also developed to predict rainfall-induced shallow landslide erosion. These layers were used in the LiDAR-based version of SedNetNZ to model contemporary suspended sediment loads as well as three future, and a retrospective ('Retro') erosion mitigation scenario for the catchment.
- The project also assessed the load reductions required to meet National Policy Statement for Freshwater Management (NPS-FM 2020)[2] suspended fine sediment (visual clarity) attribute targets, including the national bottom line (NBL) and attribute bands, and included an economic analysis of cost-effectiveness of the erosion mitigations.

Objectives

The project had five main objectives, as shown below.

- Adapt the SedNetNZ model for the dominant karst landscape to more accurately represent surface drainage, identify sink points where low-order streams terminate, and ensure hillslope erosion processes are appropriately parameterised for the catchment.
- Update the contemporary suspended sediment loads for the upper Waitomo catchment (from previous region-wide SedNetNZ modelling) [3] using the LiDAR-based version of the SedNetNZ model.
- Model future erosion mitigation scenarios, including bush retirement/afforestation, space-planted trees, and riparian retirement under three implementation scenarios.
- Assess load reductions required to meet NPS-FM 2020 attribute bands and the NBL for suspended fine sediment (visual clarity) at the 'Tumutumu' state of the environment (SOE) monitoring site ('Waitomo Stm at Tumutumu Rd') located within the catchment.
- Conduct an economic analysis to evaluate the cost-effectiveness of erosion mitigations in achieving visual water clarity targets defined by the National Objectives Framework (NOF) for suspended fine sediment.

---

[1] On 01 July 2025 Landcare Research New Zealand Ltd became the New Zealand Institute for Bioeconomy Science Ltd; Manaaki Whenua – Landcare Research operates as an internal group within this Institute, which is less formally known as the Bioeconomy Science Institute Maiangi Taiao or Bioeconomy Science Institute (BSI).

[2] Ministry for the Environment. 2020. National Policy Statement for Freshwater Management 2020. Wellington: Ministry for the Environment.

[3] See: Vale S, Smith H 2024. Application of SedNetNZ in the Waikato region to support NPS-FM 2020 implementation. Manaaki Whenua – Landcare Research Contract Report LC4432, prepared for Waikato Regional Council.

Methods

LiDAR-based SedNetNZ model description

- We generated a DSN from a sink-filled 5 m DEM using a flow direction and accumulation algorithm with a 5 ha channel initiation threshold. The DSN was subsequently edited manually to correct planform errors and further modified to represent subsurface drainage pathways characteristic of the karst system.
- We adapted SedNetNZ sub-models to incorporate LiDAR-derived DEMs, including:
  - integration of a high-resolution landslide susceptibility layer into the shallow landslide erosion sub-model
  - full implementation of the Revised Universal Soil Loss Equation (RUSLE) using LiDAR-derived topographic inputs in the surface erosion sub-model
  - implementation of a data-driven riverbank erosion sub-model
  - redefining overbank sediment deposition areas using the LiDAR-based 5 m DEM.

Erosion mitigation scenarios

- Our contemporary baseline (C2024) used recent land cover (LCDB v6; year = 2023)[4], soil conservation works, and estimated riparian fencing based on previous Catchment Environmental Monitoring (CEM) programme riparian surveys in the Waikato region. Our surface erosion sub-model also incorporates stock density data to represent the effect of livestock treading on soil erodibility.
- We also included a retrospective scenario (‘Retro’; based on LCDB v6; year = 1996) to assess the influence of erosion mitigations and land cover change since the onset of soil conservation works within the catchment.
- We modelled three future erosion mitigation scenarios (M1–M3) to represent fully implemented and matured mitigations in the upper Waitomo catchment.
  - *Mitigation scenario 1 (M1)*: included retirement/afforestation of pastoral land on slopes ≥ 35° and space-planted trees on slopes ≥ 26° and < 35°, with riparian fencing applied under Regional Plan Change 1 rules for the Waikato Regional Council.[5]
  - *Mitigation scenario 2 (M2)*: included retirement/afforestation of pastoral land on slopes ≥ 30° and space-planted trees on slopes ≥ 26° and < 30°, with 5 m riparian buffers applied to waterways (excluding first-order streams) and sinkhole (tomo) setbacks.
  - *Mitigation scenario 3 (M3)*: included retirement/afforestation of pastoral land on slopes ≥ 25°, with 5 m riparian buffers applied to waterways (excluding first-order streams) and sinkhole setbacks.

Reductions for NPS-FM visual clarity attribute bands

- We assessed proportional and absolute load reductions required to meet NPS-FM 2020 attribute bands and the NBL for the Tumutumu SOE monitoring site (‘Waitomo Stm at Tumutumu Rd’) for the contemporary baseline and three future mitigation scenarios.

---

[4] LCDB v6.0 – Land Cover Database version 6.0, Mainland New Zealand (Manaaki Whenua – Landcare Research, 2025), representing land cover circa 2023. Available at: https://doi.org/10.26060/landcareresearch/LCDBv60.

[5] See: Waikato Regional Council (WRC) 2020. Proposed Waikato Regional Plan Change 1: Waikato and Waipā River Catchments (Decisions Version). Waikato Regional Council Policy Series 2020/02. www.waikatoregion.govt.nz. (accessed September 2024).

Cost-effectiveness of erosion mitigations

- We used modelled suspended sediment loads to assess the cost-effectiveness of erosion mitigations, including bush retirement/afforestation, space-planted trees, and riparian stock-exclusion fencing and planting, implemented from 2024 to 2045.
- We estimated establishment costs (in NZ$) of the mitigations on both an undiscounted basis and discounted to a 2024 base year.
- We estimated effectiveness using modelled changes in suspended sediment loads for both overall cost-effectiveness of each mitigation scenario and the relative effectiveness of individual mitigations. Regression relationships derived from the mitigation scenarios were used to estimate the marginal contribution of individual mitigations to sediment load reduction, while catchment-scale delivery factors were used to translate source reductions to changes at the SOE monitoring site.
- We combined mitigation costs with the estimated effectiveness of the combined mitigation scenarios and individual types to calculate cost-effectiveness metrics, expressed as cost per unit reduction in suspended sediment load and cost per unit of improvement in visual clarity at the SOE site. These estimates provide both an assessment of overall cost-effectiveness of modelled mitigation scenarios and an indicative comparison of the relative cost-effectiveness of individual mitigations across the catchment.

Results

LiDAR-based SedNetNZ erosion and sediment load model for the upper Waitomo catchment

- The LiDAR-based SedNetNZ model estimated a net suspended sediment load of 5.7 kt yr^{-1} for the contemporary baseline (C2024), delivered to the Upper Waitomo catchment outlet.
- Over a multi-decadal timescale, shallow landslides contributed an estimated 61% of the suspended sediment load. Surface erosion accounted for 36%, while riverbank erosion contributed 4%.
- Under the retrospective (‘Retro’) scenario, the net suspended sediment load would be 8.5 kt yr^{-1}, 2.8 kt yr^{-1} higher than the contemporary baseline (C2024). Process contributions were similar: shallow landslides c. 63%, surface erosion 31%, and riverbank erosion 6%.
- Under the M1 scenario, total erosion load decreased by 24% relative to the contemporary baseline, reducing loads to 5.2 kt yr^{-1}. Larger reductions of 36% and 45% were achieved under the M2 and M3 scenarios, reducing total erosion loads to 4.9 and 4.6 kt yr^{-1}, respectively.

Reductions in sediment loads for NPS-FM visual clarity attribute bands

- At the Tumutumu SOE monitoring site, a 36% reduction in sediment load would be required under the contemporary baseline to achieve the NBL for visual clarity. Achieving the NOF B and A attribute bands would require reductions of 47% and 56%, respectively.
- Under full implementation of the M1, M2 and M3 mitigation scenarios, the NBL was not achieved. Additional reductions of 17%, 13% and 6%, respectively, would still be required to meet the NBL at the site, with larger reductions (35%–56%) needed to achieve the NOF A attribute band.

Cost-effectiveness of mitigations

- The three mitigation scenarios span a wide cost range, with total establishment costs of $2.5–5.6 million (undiscounted), equivalent to $2.0–4.6 million in present value at a 2%

discount rate, reflecting increasing areas of afforestation and riparian retirement across scenarios.
- The three mitigation scenarios differed in overall cost-effectiveness. M1 provided the lowest cost per unit reduction in suspended sediment load (\$1,540 t^{-1} yr^{-1}; 2% discount rate), followed by M2 (\$2,000 t^{-1} yr^{-1}) and M3 (\$2,560 t^{-1} yr^{-1}).
- Space-planted trees were the most cost-effective option for reducing suspended sediment loads and improving visual clarity, with marginal costs of \$1,190–1,210 t^{-1} yr^{-1} at a 2% discount rate and \$720–730 t^{-1} yr^{-1} at an 8% discount rate. Afforestation delivered moderate cost-effectiveness (\$2,690–2,870 t^{-1} yr^{-1} at 2%; \$1,620–1,720 t^{-1} yr^{-1} at 8%), while riparian retirement was substantially more expensive (\$12,460–14,150 t^{-1} yr^{-1} at 2%; \$7,480–8,490 t^{-1} yr^{-1} at 8%), despite achieving higher sediment reductions per hectare. The relative ranking of mitigation types remained unchanged across discount rates.

Conclusions

- The LiDAR-based SedNetNZ model estimated a contemporary suspended sediment load of 5.7 kt yr^{-1} at the Upper Waitomo outlet. Shallow landslides were the dominant sediment source (~61% of load), followed by surface erosion (~36%) and riverbank erosion (~4%). Under a retrospective scenario without erosion mitigations, the modelled load increased to 8.5 kt yr^{-1}, highlighting the importance of existing erosion control measures.
- At the Tumutumu SOE monitoring site, a 36% reduction in sediment load is required to meet the NPS-FM NBL for visual clarity. None of the mitigation scenarios achieved the NBL; further reductions of 17% (M1), 13% (M2), and 6% (M3) would still be required to meet NBL.
- Overall cost-effectiveness differed between the mitigation scenarios. M1 provided the lowest cost per unit reduction in suspended sediment load, followed by M2 and M3, reflecting the increasing costs required to achieve progressively greater sediment load reductions.
- Cost-effectiveness also varied by mitigation type. Space-planted trees were the most cost-effective option for reducing suspended sediment loads and improving visual clarity, followed by retirement/afforestation, while riparian retirement, despite achieving the highest sediment reductions per hectare, was the least cost-effective due to higher implementation costs and limited total reductions.
- Modelled sediment loads were broadly consistent with SSC–Q rating curve estimates and previous region-wide SedNetNZ modelling[6], supporting confidence in the overall magnitude of predicted loads.
- High-resolution LiDAR DEMs improved model parameterisation, stream network representation, and erosion process representation, although in this karst-dominated catchment subsurface drainage through sinkholes and cave systems introduces uncertainty in hydrological connectivity and sediment routing.

[6] See: Vale S, Smith H 2024. Application of SedNetNZ in the Waikato region to support NPS-FM 2020 implementation. Manaaki Whenua – Landcare Research Contract Report LC4432, prepared for Waikato Regional Council.

1 Introduction

Waikato Regional Council (WRC) contracted the Bioeconomy Science Institute Maiangi Taiao (BSI)[7] to model erosion and suspended sediment loads using the newly developed LiDAR-based version of the SedNetNZ model in the upper Waitomo catchment (44 km^2) (Figure 1) to support catchment management work. The project was also to assess the load reductions required to meet the National Policy Statement for Freshwater Management (NPS-FM 2020) suspended fine sediment (visual clarity) attribute targets, including the national bottom line (NBL) and attribute bands, and evaluated the cost-effectiveness of alternative erosion mitigations. This follows previous region-wide SedNetNZ modelling and the previous application of the new LiDAR-based version of SedNetNZ in four catchments from the Catchment Environmental Monitoring (CEM) programme in the Waikato region.

The upper Waitomo catchment contains the internationally recognised Waitomo cave system, where sediment deposition, stream visual clarity, and suspended sediment concentrations have been longstanding management concerns (Hawke 1976; Hoyle et al. 2012; Van Beynen and Bialkowska-Jelinska 2012). The catchment has been the focus of extensive erosion control and land management efforts since the establishment of the Waitomo Catchment Trust Board in 1993, which was formed specifically to reduce sediment and nutrient losses to the Waitomo Stream and cave network. After seven years of operation, the scheme had delivered approximately 60 km of fencing, 350 ha of commercial afforestation on former grazing land, 264 ha of native forest purchased by the Queen Elizabeth II National Trust, 360 ha of permanently retired native bush and scrubland, three dams, and three reticulated water supply schemes. By 2017, these efforts had expanded to encompass approximately 127 km of fencing and 1,235 ha of land retirement within the catchment. Since its establishment, substantial investment has continued in riparian fencing, afforestation, native vegetation retirement, and other soil conservation works.

Despite these efforts, previous analyses of the long-term monitoring record have produced mixed conclusions regarding trends in suspended sediment and the effectiveness of mitigation measures, highlighting the difficulty of separating the effects of land management from the influence of climatic variability and large storm events (Hoyle 2012; Hoyle 2014).

The catchment benefits from an extensive monitoring record, including suspended sediment monitoring at Aranui Caves since 1990 and State of the Environment (SOE) monitoring since 1993. However, a key challenge for erosion and sediment modelling in the Waitomo catchment is the presence of an extensive karst landscape, characterised by sinkholes, cave systems, and subterranean drainage networks that influence sediment transport and connectivity between erosion source areas and downstream receiving environments. Consequently, the SedNetNZ model was adapted to better represent sediment routing through the karst system and provide an assessment of contemporary sediment loads, the effectiveness of historical mitigations, and the potential benefits of future catchment management interventions.

---

[7] On 01 July 2025 Landcare Research New Zealand Ltd became the New Zealand Institute for Bioeconomy Science Ltd; Manaaki Whenua – Landcare Research operates as an internal group within this Institute, which is less formally known as the Bioeconomy Science Institute Maiangi Taiao or Bioeconomy Science Institute (BSI).

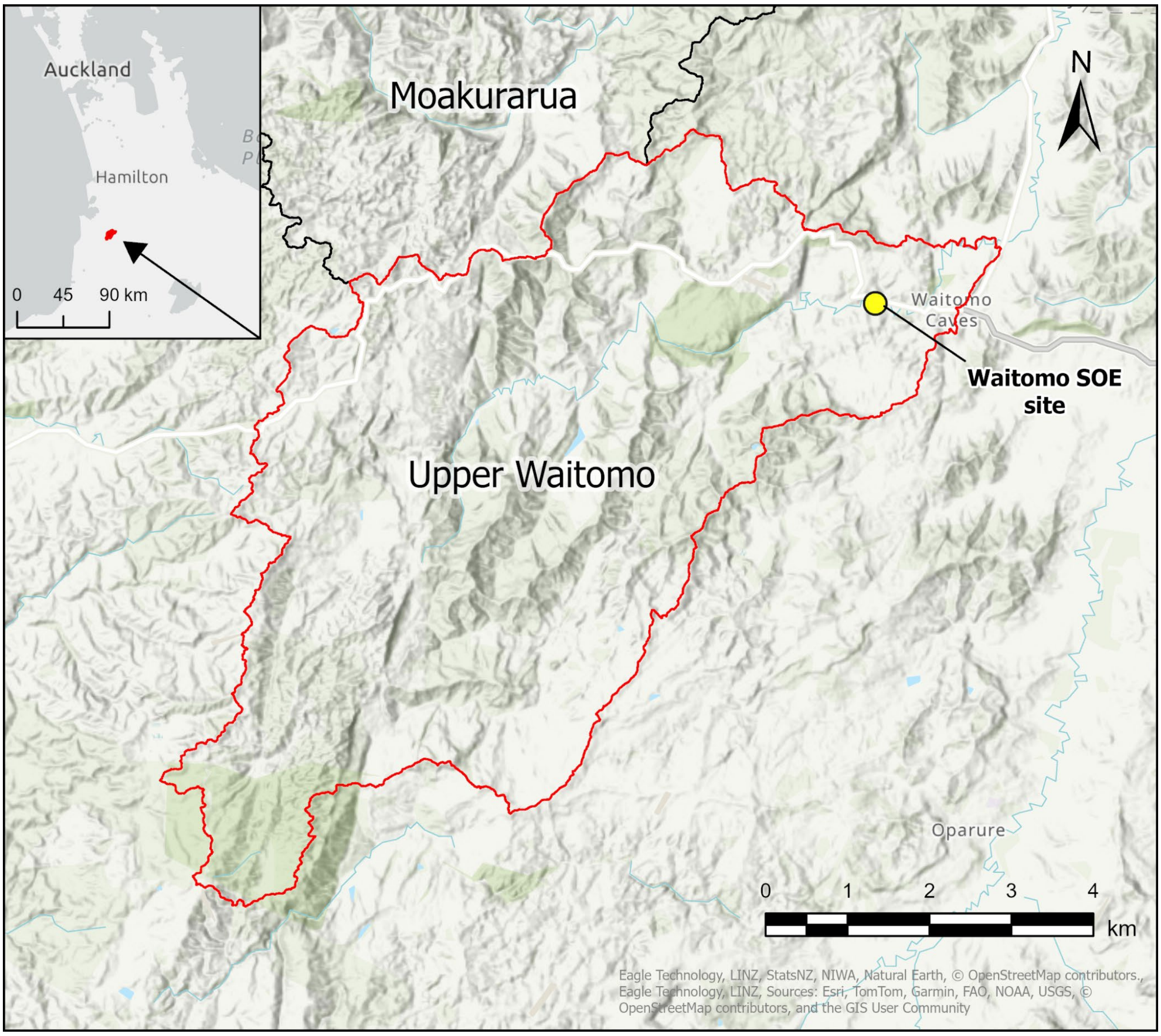

Figure 1. Upper Waitomo catchment extent used for the LiDAR-based SedNetNZ modelling, showing the Waitomo State of the Environment (SOE) monitoring site. Inset map shows the catchment location within the North Island of New Zealand.

1.1 Objectives

The project had five main objectives, as shown below.

- Adapt the SedNetNZ model for the dominant karst landscape to more accurately represent surface drainage, identify sink points where low-order streams terminate, and ensure hillslope erosion processes are appropriately parameterised for the catchment.
- Update the contemporary suspended sediment loads for the upper Waitomo catchment (from previous region-wide SedNetNZ modelling) [8] using the LiDAR-based version of the SedNetNZ model.

[8] See: Vale S, Smith H 2024. Application of SedNetNZ in the Waikato region to support NPS-FM 2020 implementation. Manaaki Whenua – Landcare Research Contract Report LC4432, prepared for Waikato Regional Council.

- Model future erosion mitigation scenarios, including bush retirement/afforestation, space-planted trees, and riparian retirement under three implementation scenarios.
- Assess load reductions required to meet NPS-FM 2020 attribute bands and the NBL for suspended fine sediment (visual clarity) at the Tumutumu SOE monitoring site monitoring site (‘Waitomo Stm at Tumutumu Rd’) located within the catchment.
- Conduct an economic analysis to evaluate the cost-effectiveness of erosion mitigations in achieving visual water clarity targets defined by the National Objectives Framework (NOF) for suspended fine sediment.

2 Background

2.1 SedNetNZ

The SedNetNZ sediment budget model represents the range of erosion processes that occur in New Zealand. These include shallow landslide, earthflow, gully, surface erosion (sheet/rill), and riverbank erosion (Dymond et al. 2016; Smith, Spiekermann et al. 2019), each with their own submodel. Hillslope erosion (shallow landslide, earthflow, gully, surface erosion) is modelled using digital elevation data derived from digital elevation models (DEMs), while bank erosion is estimated for each river segment of a digital stream network (DSN). The hillslope erosion sub-models produce raster layers of mean annual sediment yield at a common resolution, allowing outputs from different erosion processes to be combined. Estimated sediment loads generated from these processes are routed through the DSN, with losses accounted for through floodplain deposition and lake trapping, to estimate mean annual suspended sediment loads for each sub-catchment.

Two versions of SedNetNZ have been developed: the original non-LiDAR version and a newer LiDAR-based version. The earlier non-LiDAR version uses the national 15 m DEM derived from contour data and a digital stream network based on the River Environment Classification v2 (REC2; Snelder et al. 2010). The LiDAR-based version incorporates higher-resolution topography and stream data, allowing more detailed representation of the slope and DSN.

Region-wide SedNetNZ modelling for the Waikato region (Vale & Smith 2024) used the latest non-LiDAR version to produce consistent model outputs across the region, updating earlier SedNetNZ applications for the region (Palmer et al. 2013, 2015; Betts, Spiekermann et al. 2017). This version included significant updates, such as an enhanced bank-erosion model incorporating riparian woody vegetation, channel sinuosity, and bank erodibility (Smith et al. 2019, 2020); refined surface-erosion representation using spatially variable runoff and soil erodibility (Neverman et al. 2021); integration of lake sediment trapping (Neverman et al. 2021); and improved floodplain-deposition routines (Vale et al. 2021).

The Vale & Smith (2024) application to the region represented recent land cover and erosion mitigations, as well as future erosion mitigation and climate change scenarios. Backward-looking scenarios were also developed to represent past land cover and riparian fencing based on regional riparian surveys from 2002 to 2017. Sediment load reductions required to meet NPS-FM 2020 suspended-fine-sediment (visual-clarity) targets (Ministry for the Environment 2022) were evaluated for baseline and future scenarios, with and without climate-change effects.

The LiDAR-based SedNetNZ version has since been applied to update contemporary suspended-sediment loads for four CEM catchments in the Waikato region; Kaniwhaniwha (107 km^2), Karapiro (84 km^2), Matahuru (114 km^2), and Moakurarua (228 km^2) (see Vale et al. 2025a,b).

2.2 LiDAR-based SedNetNZ

The LiDAR-based version of SedNetNZ includes changes to the shallow landslide, riverbank, and surface erosion sub-models, as well as in the representation of sediment entering floodplain storage (Smith et al. 2024).

The benefits of using higher resolution LiDAR-derived DEMs in erosion and sediment load modelling may include: a) improved model parameterisation and predictive performance due to the more accurate representation of topography (e.g. slope angle, curvature); b) better representation of the stream network (e.g. channel sinuosity, channel slope, bank height); c) the ability to provide higher resolution raster layers for selected erosion processes (Smith et al. 2024).

Six specific changes in the LiDAR-based SedNetNZ compared to the current non-LiDAR SedNetNZ model are listed below.

1 Replacement of the national 15 m DEM with a LiDAR-derived 5 m DEM for use in erosion process modelling.

2 Generation of a new digital stream network and subwatershed layers using the LiDAR-derived 5 m DEM.

3 Upgrading the rainfall-induced shallow landslide erosion sub-model based on high-resolution, data-driven landslide susceptibility modelling to provide improved assessment of the spatial patterns in shallow landslide erosion based on the underpinning susceptibility model.

4 Upgrading the riverbank erosion sub-model based on data-driven modelling that draws on an expanded data set of channel planform change (increased from 77 to over 800 km of mapped channels) for use in model training.

5 Upgrading the surface erosion sub-model with the Revised Universal Soil Loss Equation (RUSLE) based on the LiDAR-derived DEM with rainfall erosivity computed from interpolated mean annual rainfall grids, while slope and runoff-contributing areas are computed from the LiDAR-derived DEM.

6 Replacing the previous representation of floodplains based on New Zealand Land Resource Inventory (NZLRI)[9] mapping at 1:63,360 scale. The extent of floodplain alongside channels where flows may go overbank and deposit sediment is now determined from the LiDAR-based 5 m DEM.

[9] NZLRI Land Use Capability 2021 – New Zealand Land Resource Inventory Land Use Capability layer (Edition 3). Manaaki Whenua – Landcare Research. Available from the LRIS Portal: https://lris.scinfo.org.nz/layer/48076-nzlri-land-use-capability-2021/

3 Methods

3.1 LiDAR pre-processing for erosion modelling

The 2021 LiDAR data set for the Waikato region was obtained from Land Information New Zealand (LINZ) in July 2024 (Land Information New Zealand 2021), clipped to the upper Waitomo catchment extents and resampled to a 5 m DEM for use in erosion modelling.

3.1.1 Digital stream network (DSN)

Digital stream network and subwatershed layers were produced for the upper Waitomo catchment. The network was generated from the sink-filled DEM using a D8 flow direction and accumulation algorithm and a 5 ha channel initiation threshold.

The DSN were used to apply the bank erosion sub-model. Therefore, the networks needed to approximate the physical extent of stream channels where fluvial scour may occur as flow is concentrated within banks (i.e. excludes zero order, un-channelised drainage lines). In earlier studies, a 5 ha stream initiation threshold was found to be optimal in the CEM catchment application (Vale et al. 2025a,b), and was applied here to the upper Waitomo catchment.

We manually refined the 5 ha digital network to correct major errors in channel planform arising from the presence of infrastructure (e.g. bridges, culverts etc.) that prevent the digital network from following the natural drainage line. We also revised parts of the network that occurred in very low-relief areas with extensive modified drainage. In these cases, the algorithm was unable to produce a representative network, so we manually digitised the network from aerial imagery.

In the Waitomo catchment, further modification was required due to its extensive karst landscape. This included identifying cave entrances and exits, mapping subsurface drainage pathways, and distinguishing between active and inactive sinkholes to determine which surface segments are hydrologically connected and able to transport sediment to downstream stream segments, ensuring the network is suitable for SedNetNZ routing. We supplemented spatial information provided by WRC, which included maps of connected entrances and exits, with expert input from members of the New Zealand Speleological Society, whose local knowledge of the Waitomo cave system helped identify watersheds with known subterranean connections and link them to the appropriate downstream subwatershed, required for sediment routing.

Differences in channel network length between the LiDAR DEM-derived network and the REC2 digital network reflect both differences in channel initiation thresholds and channel sinuosity (Figure 2). The LiDAR-derived network provides a better representation of channel planform geometry, capturing greater sinuosity and resulting in a longer total stream length (81 km compared with 68 km for the REC2 network). In the upper Waitomo catchment, the LiDAR-based network also represents surface drainage patterns more accurately, particularly in karst terrain where stream flow disappears into sinkholes, leading to some subwatersheds without surface stream segments. To maintain downstream connectivity for sediment routing, known cave entrances, exits, and subsurface connections were used to link affected subwatersheds within the digital network, allowing sediment to be routed through the karst system in the same way as surface channels.

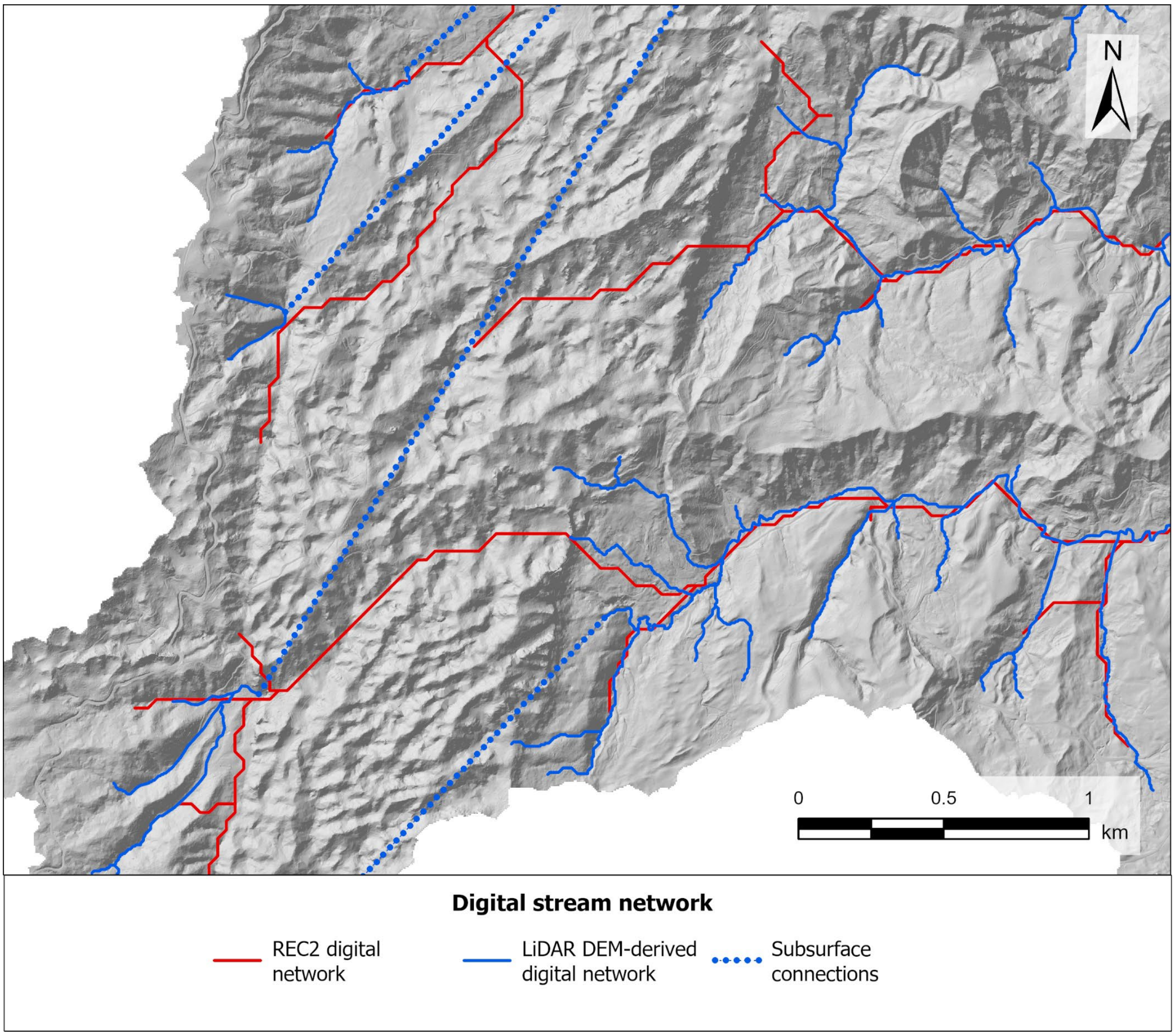

Figure 2. Example of the new LiDAR DEM-derived digital network (blue) compared to the previous REC2 digital network (red), showing improved planform accuracy and stream representation as well as indicative subsurface connections. The LiDAR-based network more accurately represents surface drainage patterns, particularly in karst areas where stream flow disappears into sinkholes.

3.1.2 Shallow landslide susceptibility

The LiDAR-based version of SedNetNZ integrates high-resolution landslide susceptibility with the shallow landslide erosion sub-model to estimate landslide-derived sediment loads (described in Section 3.2.1). This development requires spatial prediction of shallow landslide susceptibility using a statistical susceptibility model (Smith et al. 2024). In this section, we describe the approach to modelling rainfall-induced shallow landslide susceptibility using the LiDAR-derived DEM in the upper Waitomo catchment. Landslide susceptibility modelling involved: a) assembling a dataset comprising landslides located in areas with LiDAR coverage; b) applying a logistic regression model to relate landslide presence/absence to topographic, geological, and land-cover variables and evaluating model performance; and c) predicting landslide susceptibility at 5 m resolution from the regression model.

As part of step (a), the data set available for susceptibility modelling in the present study comprises shallow landslides (over *n* = 123,000) assembled from mapping areas in the Hawke’s Bay, Gisborne, Greater Wellington, and Waikato regions that overlap with existing LiDAR coverages (Table 1). This combined data set exceeds that previously used by Smith et al. (2024) with the addition of landslide data from the Waikato region. Non-landslide locations were randomly selected from within these landslide mapping areas to produce a balanced sample comprising equal numbers of landslide and non-landslide points for statistical modelling (Smith et al. 2021).

As part of step (b), binary logistic regression (BLR) was used to classify landslide and non-landslide locations. BLR is a statistical method used to predict the probability of a binary outcome, such as landslide presence or absence, from one or more explanatory variables. This type of regression requires spatial data corresponding to landslide/non-landslide locations for variables that may influence susceptibility. Our analysis drew on spatial data sets for elevation (5 m LiDAR-derived DEM), land cover (LCDB v5)[10] and rock type (NZLRI[11]; Newsome et al. 2008). Slope angle (continuous variable), aspect (categorical variable with 8 classes), profile (categorical: convex, concave, planar) and planform curvature (categorical: convergent, divergent, planar) were also derived from the DEM. These input variables were selected for use in statistical modelling because: a) there is a potential physical basis for how each variable may influence landslide susceptibility (Smith et al. 2021); b) model inputs can be derived for all areas.

Table 1. Summary information for the landslide mapping areas with LiDAR coverage contributing data to the shallow landslide data set used for susceptibility modelling

Location	Study area (km^2)	Period	Number of landslides	Imagery sources (resolution)	Data source
Southern Hawke's Bay	175	Event (2011)	27,170	Orthorectified aerial photography and Worldview-2 (0.4 m)	Smith et al. (2021)
Northern Hawke's Bay and Gisborne	3,162	Multi-event (2022)	45,879	Orthorectified aerial photography (0.3 m) and Pleiades (0.5 m)	Betts et al. (2023)
Wairarapa, Greater Wellington	843	Multi-event (2005-10)	43,069	Orthorectified aerial photography (0.4 m)	Spiekermann et al. (2021)
Wairamarama, Waikato	178	Event (2017)	7,704	Pleiades-1A and GeoEye-1 (0.5 m)	Smith et al. (2021)

BLR has been widely applied internationally for landslide susceptibility analysis (Reichenbach et al. 2018). This regression is a type of generalised linear model (GLM) that uses a logistic function with a binary dependent variable (landslide presence/absence). It relates the probability (P) of landslide presence (Y = 1) to the spatial explanatory variables (x_1, x_2,…x_n) where β_0, β_1, β_2…β_n are fitted constants (Equation 1):

$$P(Y=1) = \frac{1}{1 + e^{-(\beta_0 + \beta_1 x_1 + \beta_2 x_2 \dots \beta_n x_n)}} \qquad (1)$$

Model predictive performance was assessed using *k*-fold cross-validation whereby we tested the model by repeatedly training it on part of the data and checking how well it predicted the remaining

[10] Land Cover Database v5.0 (LCDB v5) – Mainland New Zealand. Manaaki Whenua – Landcare Research (2020). Available from the LRIS Portal: https://lris.scinfo.org.nz/layer/104400-lcdb-v50-land-cover-database-version-50-mainland-new-zealand-deprecated/

[11] NZLRI Land Use Capability 2021 – New Zealand Land Resource Inventory Land Use Capability layer (Edition 3). Manaaki Whenua – Landcare Research. Available from the LRIS Portal: https://lris.scinfo.org.nz/layer/48076-nzlri-land-use-capability-2021/

data. Accordingly, the data set comprising landslide and non-landslide locations was randomly shuffled and then split into k = 5 folds, where k – 1 folds were used for model training and each remaining fold (20% of the data) was used once for testing. Sensitivity to the location of non-landslide points was also tested by repeating the randomised placement of absence points five times. The procedure was repeated to produce a total of 100 data partitions for model fitting and testing.

We evaluated model classification performance (i.e. landslide versus non-landslide) using receiver operating characteristic (ROC) curves and we calculated the area under the curve (AUC) based on the 100 iterations. ROC curves and AUC values are widely used in the landslide susceptibility literature to assess model performance (Reichenbach et al. 2018).

The ROC curves plot the true positive rate ($TPR = \frac{True\ Positive}{True\ Positive + False\ Negative}$) versus the false positive rate ($FPR = \frac{False\ Positive}{True\ Negative + False\ Positive}$) providing an indication of sensitivity (probability of detection) versus 1 – specificity (where specificity refers to the true negative rate) (Conoscenti et al. 2016). An AUC value of 0.5 corresponds to performance no better than a random guess, while a value of 1 indicates perfect classification. Model performance is generally considered 'fair' above 0.7, 'good' between 0.8-0.9, and 'excellent' above 0.9 (Carter et al. 2016). In the present version, the BLR model achieved a median AUC of 0.9 in cross-validation.

As part of step (c), the fitted BLR model was used to generate a high-resolution (5 m) map of shallow landslide susceptibility for the upper Waitomo catchment. The model was applied to spatial layers of the explanatory variables (e.g. elevation, slope, curve, land cover and rock type) to predict the probability of landslide susceptibility. The resulting susceptibility map, expressed as a spatial probability (ranging from 0 to 1), was then used as an input to the shallow landslide sub-model that forms part of the LiDAR-based SedNetNZ (see Section 3.2.1).

3.2 LiDAR-based SedNetNZ model description

SedNetNZ computes a mean annual suspended sediment budget for the subwatershed draining to each segment in the LiDAR DEM-derived digital stream network. Each sediment budget comprises erosion process (i.e. surface, shallow landslide, gully, earthflow, and riverbank) sediment loads delivered to the stream segment minus any sediment entering floodplain storage (see Fig. 2 in Dymond et al. 2016). The resulting net suspended sediment load is then routed to the next downstream segment and through the network to the catchment outlet, while accounting for deposition in lakes.

We produced predictions of mean annual surface and shallow landslide erosion using the LiDAR DEM–based sub-models on a 5 m grid, while bank erosion was estimated for each stream segment in the digital network. Earthflow and gully terrains were not present in the upper Waitomo catchment; therefore, the corresponding sub-models were not implemented or described below. Net suspended sediment loads and sediment yields were computed for each subwatershed draining to a digital stream segment for the upper Waitomo catchment.

3.2.1 Shallow landslide sub-model

Shallow landslides are considered the most common form of erosion in New Zealand hill country (Basher 2013; Eyles 1983; Phillips et al. 2021). Shallow landslides are typically < 2 m deep and individual source areas (scars) are generally small (median size 50–100 m^2) (Betts, Basher et al. 2017; Smith et al. 2021). Landslide-triggering storm events occur episodically and thus the contribution of shallow landslides to suspended sediment loads will exhibit significant inter-annual variation. For this reason, SedNetNZ averages across a multi-decadal period to estimate the longer-term contribution of shallow landslides to mean annual suspended sediment loads rather than attempting to estimate the contribution for any given year.

In SedNetNZ, the mass of soil eroded by shallow landslides and delivered to the stream network per square kilometre per year (EL) is estimated by:

$$EL = \rho \times SDR \times d_l \times f(s) \tag{2}$$

where ρ is the bulk density of soil (t m^{-3}), SDR is the sediment delivery ratio, d_l is the mean depth of landslide failure (m), and $f(s)$ is the expected area of landslide scars per square kilometre per year at slope angle s (m^2 km^{-2} yr^{-1}) for terrain under grass cover.

Bulk density (ρ) is set to 1.5 t m^{-3} (Dymond et al. 2016); d_l is set to 1 m (Page et al. 1994; Reid & Page 2002; Betts, Basher, et al. 2017; Phillips et al. 2021); and SDR values are 0.5 in hill country and 0.1 in hard rock mountain areas, reflecting the tendency for landslides in hard rock mountainous areas to contain a larger proportion of rock (Dymond et al. 2016).

In the LiDAR-based version of SedNetNZ, the estimation of the landslide-eroded area term ($f(s)$), has been updated using empirical landslide area–slope relationships derived from approximately 70 years of multi-temporal landslide mapping in the Manawatū catchment (Dymond et al. 2016; Betts, Basher et al. 2017; Smith et al. 2024). Separate relationships were developed for grass cover on soft rock terrain and woody cover on hard rock terrain from the Manawatū study areas (Betts, Basher et al. 2017). Slope was derived from photogrammetrically derived 2 m DEMs (in the absence of LiDAR) and resampled to 5 m for consistency with the Waikato 5 m DEM. These revised landslide-eroded area versus slope relationships (Figure 3b) replaced the single landslide-slope relationship originally based on the national 15 m DEM (Dymond et al. 2016); see Figure 3a. We derived the soft rock landslide-slope relationship using data from landslide mapping of hill country areas under mostly grass cover (Betts, Basher et al. 2017). The hard rock relationship was based on landslide mapping data from greywacke ranges under woody vegetation (Fuller et al. 2016). Therefore, the lower landslide eroded area per 1° slope bin for hard rock terrain in Figure 3b reflects the influence of both woody cover and rock type on landslide erosion.

The predicted landslide-eroded area for each 1° slope bin ($f(s)$) was then distributed spatially using the modelled landslide susceptibility (Section 3.1.2). The 2023 land cover from LCDB v6.0 was reclassified into woody cover on hard rock areas and grass cover on non-hard rock terrain, and this reclassified cover layer was used to predict landslide susceptibility for each domain. The resulting susceptibility layer was then used to spatially allocate the predicted landslide-eroded area using a percentile matching approach (Smith et al. 2024). Within each domain, pixel-wise landslide susceptibility and slope values were ranked, and the predicted landslide-eroded area for each 1° slope bin was assigned to the corresponding landslide susceptibility-ranked pixels. This preserved the total landslide-eroded area predicted by the empirical landslide–slope relationships while preferentially allocating erosion to the highest susceptibility locations, producing a 5 m raster of shallow landslide erosion. In this upper Waitomo application, percentile matching parameters derived from the CEM catchments (Vale et al. 2025a,b), which represent a broader range of terrains, were used to apply the matching within the upper Waitomo catchment.

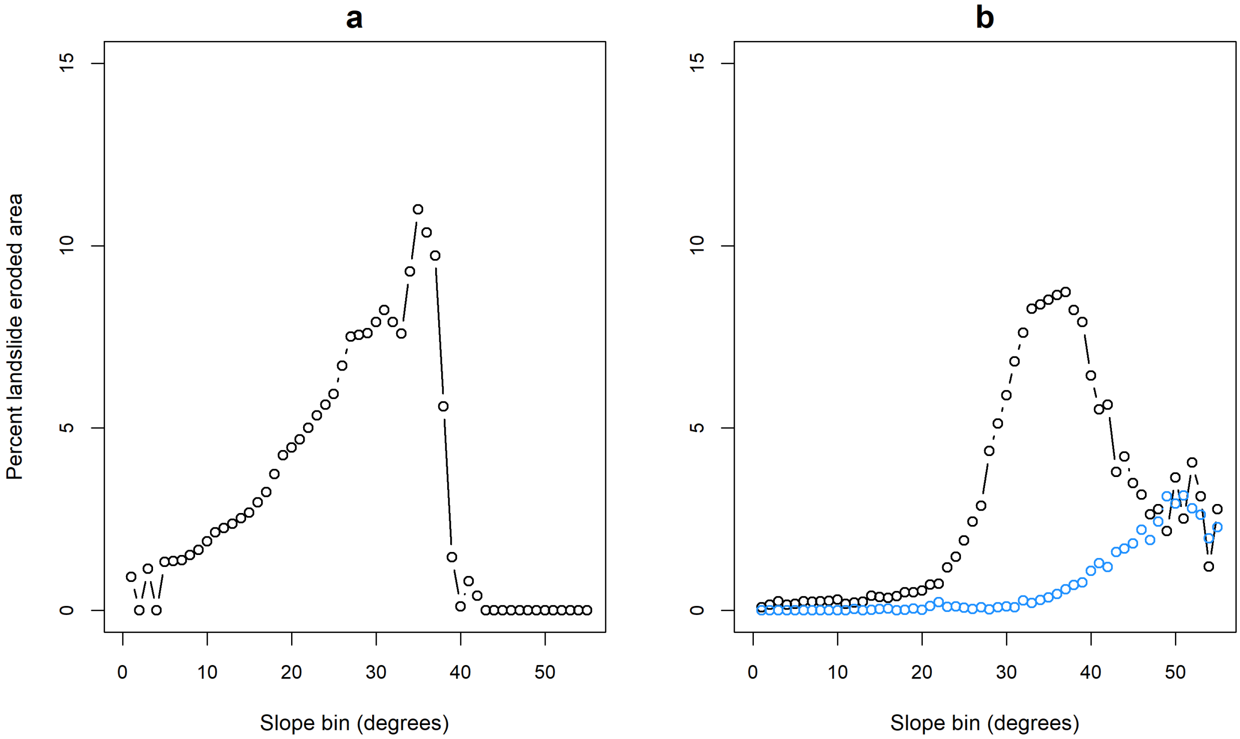

Figure 3. Plots of landslide-eroded area (expressed as a percentage of each slope bin) per 1° slope bin for: a) national 15 m DEM (previous SedNetNZ model; Dymond et al. 2016); b) 5 m DEM for soft rock under grass (black circles) and hard rock under woody vegetation (blue circles) terrain based on multitemporal polygon mapping (70-year interval) of shallow landslide erosion in the Manawatū catchment. (Source: Reproduced from Smith et al. 2024, Figure 9.)

Permanent woody cover was estimated to reduce shallow landslide erosion by 90% compared with pasture (see Basher 2013; Dymond et al. 2016; Phillips et al. 2020; Smith et al. 2023); while we applied an estimated 80% reduction for exotic plantations over multiple rotations (first applied in Vale et al. 2021). The lower reduction estimated for plantation versus permanent forest recognises the effectiveness of forest cover for reducing shallow landslides (Marden 2012; Smith et al. 2023) for much of the rotation while acknowledging the period spanning several years between harvest and canopy closure of the replanted crop during which there is an increase in susceptibility to shallow landslide erosion (Phillips et al. 2018, 2024). Because the empirical landslide–slope relationships ($f(s)$) were derived separately for grass-covered soft rock terrain and permanent woody-covered hard rock terrain (Figure 3), these vegetation reductions were only applied to soft rock terrain where permanent woody vegetation was present, as the influence of permanent woody vegetation is already incorporated within the hard rock calibration. Conversely, landslide erosion in hard rock areas under non-woody vegetation and exotic forest was increased by an inverse proportion to represent the higher erosion rates expected in the absence of permanent woody cover.

To prevent small amounts of landslide erosion from occurring on very low slope land in this sub-model, we applied a slope threshold of 6° below which landslide erosion was deemed negligible. This threshold corresponds to an approximate susceptibility value of 0.01, representing the land least susceptible to instability. We did not model landslide susceptibility for LCDB-mapped urban areas due to insufficient data, thus landslide erosion was not estimated for these areas.

3.2.2 Surface erosion sub-model

In the LiDAR-based version of SedNetNZ surface erosion (sheet and rill erosion resulting from rainfall impact and overland flow) is estimated using the Revised Universal Soil Loss Equation (RUSLE; Renard et al. 1997), in place of the New Zealand Universal Soil Loss Equation (NZUSLE; Dymond et al. 2010) used in earlier applications. The RUSLE allows explicit representation of rainfall erosivity and improved characterisation of topographic controls using high-resolution LiDAR-derived terrain data.

The RUSLE and the earlier Universal Soil Loss Equation (USLE) (Wischmeier & Smith 1978) are empirical models developed using an extensive erosion data set obtained from plot measurements on predominantly agricultural land (Renard et al. 1997). The USLE/RUSLE was originally developed in the United States and has since been widely applied globally, including in New Zealand using the national 15 m DEM (Donovan 2022).

As RUSLE represents gross surface erosion and cannot be used to directly quantify the net sediment loads delivered to streams. We therefore use a sediment delivery ratio (SDR = 0.1) that approximates the previously calibrated NZUSLE to estimate the total net load delivered to the stream network from surface erosion. The NZUSLE was originally calibrated with measurements of surface erosion rates from across New Zealand (Dymond et al. 2013, 2016). We do not have LiDAR coverages that overlap with the calibration data and thus cannot apply an updated calibration to the LiDAR-based RUSLE estimate of surface erosion.

Therefore, mean annual surface erosion using RUSLE was estimated as:

$$ES = R \times K \times LS \times C \times SDR \tag{3}$$

where (ES) is surface erosion (t km^{-2} yr^{-1}), R is rainfall erosivity, K is soil erodibility factor (dimensionless), LS is the combined slope length and slope steepness factor (Equations 4-7), and C represents the impact of vegetation cover (dimensionless) assigned according to land-cover class using values previously adopted in SedNetNZ applications (e.g. bare ground = 1.0, pasture = 0.01, forest and scrub = 0.005).

The LS factor was derived from the 5 m LiDAR DEM using the approach of Desmet and Govers (1996) and Renard et al. (1997), which accounts for upslope contributing area and flow convergence:

$$L = \frac{(A\ +\ D^2)^{m+1} - A^{m+1}}{D^{m+2}\ \times\ x^m\ \times\ 22.13^m} \tag{4}$$

where L is the slope length factor for a given raster cell (pixel), A is the upstream catchment area (m^2) at the cell inlet, D is the raster cell width (m), m is the slope length exponent, and x = sin a + cos a, with α being the slope aspect.

The slope length exponent, m, was calculated based on the rill to inter-rill ratio, β, and the slope gradient, θ (Foster et al. 1977; McCool et al. 1989, cited in Renard 1997) and shown in Equations 5 and 6:

$$\beta = \frac{\sin\theta / 0.896}{3\ \times (\sin\theta)^{0.8}\ +\ 0.56} \tag{5}$$

$$m = \frac{\beta}{1 + \beta} \tag{6}$$

The slope steepness factor S was calculated following Renard et al. (1997):

$$S = \begin{cases} 10.8 \times \sin\theta + 0.03 & with\ sp\ < 9\% \\ 16.8 \times \sin\theta - 0.5 & with\ sp\ \geq 9\% \end{cases} \tag{7}$$

where (sp) is slope gradient (%).

The soil erodibility factor (K) was estimated using the spatially variable approach of Neverman et al. (2021), which adapts the K factor equations of Wang et al. 2001 and Yang et al. 2018, using Fundamental Soil Layer (FSL) attributes:

$$K = \frac{2.1(12 - OM)M^{1.14}10^{-4} + 3.25(SS - 2) + 2.5(PP - 3)}{7.59 \times 10} \tag{8}$$

where OM is the soil organic matter content, M is the particle size parameter, SS is the soil structure code, and PP is the soil profile permeability code. Six PP classes were adapted from Rosewell & Loch (2002). The soil structure code was set at SS = 2 because the FSL has insufficient data on soil structure to relate to the SS classes used for calculating K. Neverman et al. (2021) found the magnitude of K was not sensitive to the choice of SS class value.

The particle-size parameter (M) was calculated as a function of the proportion of silt and clay:

$$M = Silt(100 - Clay) \tag{9}$$

where $Silt$ and $Clay$ are the percentage of silt and clay in the soil, respectively.

$Silt$ was limited to a range of 15%–70%, and OM was capped at 4% to fit the nomograph of Wischmeier et al. (1971) for organic soils. Where there was no FSL information available to calculate a spatially varying K factor, a uniform value of 0.25 was used (Dymond et al. 2010).

Rainfall erosivity (R) represents the erosive power of rainfall at the soil surface (Nearing et al. 2017). We estimated R using the New Zealand rainfall erosivity relationships developed by Klik et al. (2015), which relate rainfall erosivity to mean annual rainfall within different climatic regions. The previous NZUSLE rainfall term (aP^2), based on mean annual rainfall (Leathwick et al. 2003), was replaced with a spatial rainfall erosivity surface derived from mean annual rainfall for the period 1981–2010. This provides a more direct representation of the influence of rainfall characteristics on surface erosion rates.

Surface erosion was predicted on a 5 m grid across the catchment. Channel cells identified from the LiDAR-derived digital stream network were excluded from calculations, ensuring that only hillslope-derived surface erosion was represented. The resulting raster represents mean annual sediment yield from surface erosion and is produced at the same spatial resolution as the other hillslope erosion sub-models, allowing erosion-process outputs to be combined within the SedNetNZ sediment budget model.

Stocking density–adjusted soil erodibility factor

The effect of livestock treading and grazing on surface erosion was incorporated into the LiDAR-based version of SedNetNZ through an adjustment to the surface erodibility factor (K factor in Equation 3), using the approach of Donovan and Monaghan (2021). This method was first implemented in SedNetNZ for the Waikato CEM catchments (Vale et al. 2025a,b). This approach represents soil damage due to livestock activity via changes in soil permeability (ΔP_{tr}; see Equation 10) and structure (ΔS_{tr}; see Equation 11), which are components of the *K*-factor. We parametrised the changes in permeability and structure based on grazing intensity, soil moisture, clay content, and soil susceptibility to compaction and pugging according to the following equations:

$$\Delta P_{tr} = 1 + \left(p - \left(p\ (1 - 0.05\ (hd^{0.5}))e^{-0.5\ i\omega_c}\right)\right) \quad (10)$$

$$\Delta S_{tr} = 1 + \left(p - \left(p\ \left(1 - 0.05\ \left(hd^{\{0.5\}}\right)\right)e^{-0.5\ i\omega_p}\right)\right) \quad (11)$$

where ΔP_{tr} and ΔS_{tr} reflect the 'soil damage' represented via the soil permeability (PP) and structural vulnerability (SS) parameters in the RUSLE *K*-factor (Equation 8); p is normalised average stock hoof pressure (kPa/kPa) with values of 0.38 for sheep, and 0.7 for cattle (Fig. 2A in Donovan & Monaghan 2021); h reflects the grazing history (successive years), set to a constant 6 years, the longest reported by Donovan and Monaghan 2021 (see their Fig. 2B); d is the grazing duration, expressed as the fraction of time across the season (0-1, unitless). A value of d =1 was applied, reflecting consistent seasonal grazing practices; i is grazing intensity (relative stock unit, RSU m^{-2}) as derived from Equation (12), and ω_c and ω_p are soil susceptibility factors for compaction and pugging, respectively (Equations 13 & 14).

The value of d =1 was based on Donovan and Monaghan (2021), reflecting consistent grazing durations at the seasonal timescale, which align with typical pasture management practices in New Zealand. This has some justification given the age of the underlying AgriBase® (AssureQuality 2020) data is at least three years old, and both land use changes and the average lifespan of a farm typically occur over much longer time frames. Moreover, soil damage appears to be relatively insensitive to variations in h, particularly at higher grazing intensities (Donovan & Monaghan 2021).

Donovan and Monaghan (2021) describe grazing intensity (i) as a function of grazing density (g, head/ha) and a relative stock unit (RSU) constant (c). While Donovan and Monaghan (2021) provide typical RSU constants (c), they emphasised locally informed values are preferred to refine RSU values for specific stock types. We followed the same approach as the CEM catchment application (Vale et al. 2025a,b), and were provided AgriBase® stock numbers from WRC to estimate local stock unit densities (SUD) and these were substituted for gc in Equation 12:

$$i = \frac{gc}{10{,}000} = \frac{SUD}{10{,}000} \quad (12)$$

Compaction susceptibility (ω_c) and pugging susceptibility (ω_p) were modelled according to the Equations 13 and 14:

$$\omega_c = -0.003\ \phi\big(75\sigma - 20(\phi + 1)\big)^2 + 8\phi + 2 \quad (13)$$

$$\omega_p = 1 - e^{-500\phi\left(max\left(0,\ \sigma^3 - 0.25\phi\right)\right)^2} \quad (14)$$

where, (ϕ) is the clay content (0–1) from the FSL clay value in Equation 9; and σ is the soil water content (SWC). In the absence of high-resolution spatial data, Donovan and Monaghan (2021; their Fig. 2D) estimated seasonal averages for SWC using data from New Zealand soil measurements (Curran-Cournane et al. 2011; Laurenson et al. 2016). We used the mean of these seasonal averages to derive an annual estimate (σ = 0.325).

3.2.3 Riverbank erosion sub-model

Riverbank erosion was estimated using the LiDAR-based riverbank erosion sub-model developed by Smith et al. (2024). Earlier applications of SedNetNZ estimated bank erosion using empirical relationships between mean annual flood and bank migration rates (Dymond et al. 2016), while subsequent refinements incorporated additional controls on bank erosion processes (Smith, Spiekermann et al. 2019). The present LiDAR-based implementation adopts the latest riverbank erosion sub-model, which uses machine-learning predictions of bank migration rates, LiDAR-derived estimates of bank height, and an estimate of net bank erosion to calculate the mean annual suspended sediment load contributed by riverbank erosion for each stream segment in the digital stream network (DSN).

$$B_j = \rho \times M_j \times H_j \times L_j \tag{15}$$

where B_j is the total eroded mass for the j^{th} stream segment (t yr^{-1}), ρ is the bulk density of the bank material (t m^{-3}), M_j is the bank migration rate (m yr^{-1}), H_j is the mean bank height (m) and L_j is the length (m) of the j^{th} stream segment.

The predicted mass of material eroded from riverbanks represents the gross contribution of sediment supplied to the channel. However, some of this material is subsequently redeposited on banks, bars, and within the channel bed. Consequently, estimation of suspended sediment loads requires an assessment of net bank erosion rather than gross bank erosion alone.

Bank migration rates

Bank migration rates were predicted using the random forest (RF) model developed by Smith et al. (2024). The RF model was trained using an expanded data set of reach-averaged lateral bank migration rates derived from mapping channel planform change from repeated aerial imagery in the Hawke’s Bay and Greater Wellington regions. This mapping increased the length of channel available for model training from 77 km to more than 800 km.

The RF model predicts bank migration rates using variables describing channel hydraulics, geometry, confinement, bank erodibility, and riparian vegetation. Smith et al. (2024) evaluated four candidate models and found that the RF model produced the lowest fitting and prediction errors. The fitted model achieved a mean (R^2) of 0.87, with fitting errors of RMSE = 0.15 m yr^{-1} and MAE = 0.06 m yr^{-1} and prediction errors of (RMSE = 0.31 m yr^{-1}; MAE = 0.14 m yr^{-1}). The RF model also outperformed previous bank erosion modelling approaches and was therefore adopted for the LiDAR-based version of SedNetNZ.

For application in the upper Waitomo catchment, predictor variables were derived from the LiDAR-based DSN and 5 m DEM. Mean annual flood (MAF) was estimated from modelled mean annual discharge using a fitted power relationship developed for the Waikato region ($MAF = 26q^{0.61}$; R^2 = 0.97; n = 35), where (q) is mean annual discharge (m^{-2} s^{-1}) (Vale & Smith 2024). Mean annual discharge for the REC2 network was previously estimated using an empirical water balance model (Woods et al. 2006; Elliott et al. 2016). These discharge estimates were converted to runoff and reapplied to the LiDAR-based DSN using the upstream contributing area of each stream segment.

Channel slope, channel sinuosity, and valley confinement were computed from the LiDAR-based DSN and 5 m DEM. Soil texture classes compiled from the Fundamental Soil Layer (FSL) were used to represent bank erodibility. Riparian woody vegetation was estimated using a canopy height model (CHM) generated by differencing the LiDAR-derived digital surface model (DSM) and DEM, with vegetation greater than 2 m in height classified as woody vegetation. This high-resolution

CHM replaced the Landsat-derived woody vegetation layer used in previous regional SedNetNZ applications and provided improved representation of riparian vegetation characteristics. The fitted RF model was then applied to predict reach-average bank migration rates for all stream segments in the upper Waitomo catchment.

Bank height

Mean bank height was estimated directly from the LiDAR-derived 1 m DEM. Bank heights were derived from transects generated perpendicular to the DSN at 50 m intervals. Transect widths varied according to mean discharge and the inverse of mean lateral slope (as a proxy for valley confinement) to approximate variations in bankfull channel width (Smith et al. 2024).

This LiDAR-based approach captures local variations in channel form and bank morphology that are not represented by the simpler discharge-based relationships used in earlier SedNetNZ applications. Validation against manually measured bank heights in the Hawke's Bay region showed a substantial improvement in predictive performance, increasing the coefficient of determination R^2 from 0.40 to 0.66 relative to the previous approach (Smith et al. 2024).

Net bank erosion

Estimating the net contribution of bank erosion to suspended sediment loads requires information on the redeposition and storage of eroded bank material on banks, within the channel bed; or on the lateral accretion of material on bars with channel migration. Such information is not widely available.

Subsequently, net bank erosion was estimated from extensive channel planform mapping in the Hawke's Bay region for comparison with the previous Waipaoa-based estimate (Smith et al. 2024). This planform mapping identified areas of both erosion and accretion within channels for each digital stream segment which were converted to mean annual rates of reach-average lateral erosion or accretion (m yr^{-1}). Average erosion and accretion volumes per segment per year were then approximated using the average of the maximum and minimum mapped bank heights per transect, respectively. This planform mapping analysis assumed that, for laterally migrating channels, the outer eroding bank is typically higher than the opposite accreting bank. In practice, bank heights may vary between erosion and accretion zones, while some reaches may experience erosion or accretion along both banks. Nonetheless, this assumption provided a first-order approximation for estimating net bank erosion based on a significantly larger data set (805 km of channel length) for comparison with the previous estimate based on 44 km of mapped channel length in the Waipaoa catchment.

Net bank erosion as a proportion of gross bank erosion was estimated at 0.28 based on the channel planform and bank height mapping data from Hawke's Bay (Smith et al. 2024). This is comparable to the 0.20 estimate used in previous SedNetNZ modelling. While both estimates are subject to considerable uncertainty, their consistency suggests that these values may provide a reasonable approximation for determining net bank erosion in the absence of repeated LiDAR surveys.

Suspended sediment loads from bank erosion

The RF sub-model was fitted 100 times (mean R^2 = 0.87) using all available bank migration data and the resulting mean predicted bank migration rate per stream segment was used in the upper Waitomo catchment. We then combined these mean predictions of bank migration rates with the

LiDAR-based estimates of mean bank height per stream segment, and the revised estimate of net bank erosion to estimate mean annual net suspended sediment load from bank erosion per stream segment in each catchment.

3.2.4 Sediment routing and floodplain storage

SedNetNZ estimates the mean annual suspended sediment load from the combined erosion process loads delivered by each erosion process to the DSN. The 5 m raster-based hillslope erosion estimates (i.e. shallow landslide and surface erosion) are aggregated within each LiDAR-derived subwatershed to calculate the total sediment load delivered to the corresponding stream segment. Riverbank erosion is estimated directly for each stream segment. This sediment is then routed through the network to the coast. In the application of SedNetNZ to the Waikato region (Vale & Smith 2024), the revised floodplain deposition algorithm was applied to estimate the amount of sediment entering floodplain storage along the stream network based on upstream loads (Vale et al. 2021).

In the revised algorithm, we allocate the total sediment entering floodplain storage among subwatersheds according to a weighting based on both floodplain stream length and the accumulated upstream sediment load. Consequently, subwatersheds with longer floodplain-adjacent stream lengths and larger accumulated sediment loads receive a greater proportion of the total floodplain storage. The mass of sediment (t yr^{-1}) entering floodplain storage in the ith subwatershed (F_i) is calculated as shown in Equation 16:

$$F_i = pS_t \frac{L_i accS_i{}^2}{\sum L_i accS_i{}^2} \tag{16}$$

where p is the proportion of the sediment load generated by hillslope erosion per lake or sea-draining catchment that is deposited on floodplains in the catchment, set to 5% based on previous SedNetNZ parameterisation carried out in the Manawatū (Dymond et al. 2016), S_t is the total sediment load (t yr^{-1}) generated by hillslope erosion per lake or sea-draining catchment, L_i is the segment length (m) on floodplain in the ith subwatershed, and $accS_i$ is the total accumulated (upstream) sediment load from hillslope erosion (t yr^{-1}) in the ith subwatershed.

We use the LiDAR-derived 5 m DEMs for the upper Waitomo catchment to identify the extent of floodplains along the digital stream network. We did not seek to model the area of floodplain inundated by the largest flood on record. Instead, we represented the length of channel where flows may go overbank and deposit sediment on floodplains on average over a multi-decadal period (i.e. L_i in Equation 16). Therefore, we defined floodplains as areas of low slope land adjacent to the active channel which may be inundated by the average annual maximum flow within each subwatershed.

Smith et al. (2024) estimated the depth of the average annual maximum flow across stream orders (for orders 1–8) using the annual maximum flow from 77 water level gauges in Hawke's Bay, with a mean record length of 27 years. Based on this analysis, they estimated maximum floodplain height above the channel ranged from 1–5 m depending on the stream order. They used these values to identify subwatersheds where sediment may enter floodplain storage. We applied the same criteria to determine the floodplain extent in the upper Waitomo catchment, using height above nearest drainage (HAND) to identify floodplains. The stream bed and banks were excluded from the floodplain extent using a 7.5 m buffer either side of the streamlines (i.e. for a total width of 3 pixels), and a slope threshold of 5°.

SedNetNZ includes a lake sediment trapping component to account for sediment storage within lakes. Where lakes are present, a lake-specific sediment passing factor (SPF) is applied using an adaptation of Gill's (Gill 1979) approximation of Brune's (Brune 1953) trap efficiency (the inverse of passing factor) curve for medium sediment, as in in Equation 17:

$$SPF = 1 - \frac{V/_I}{1.02\left(V/_I\right) + 0.012} \tag{17}$$

where V is the lake volume, and I is the annual inflow to the lake.

No lakes occur within the upper Waitomo catchment and therefore no lake sediment trapping was simulated in the present application. However, the equation is provided for completeness, as it forms part of the standard SedNetNZ sediment-routing framework.

3.3 Model simulations

3.3.1 Scenario overview

Contemporary baseline scenario

The contemporary baseline scenario (C2024) represents recent land cover (LCDB v6.0, mapping year = 2023)[12] and erosion mitigations (soil conservation works) completed to date by WRC and landowners within the catchment, based on data provided by WRC.

We estimate the proportional extent of riparian fencing for each segment in the DSN from existing riparian retirement spatial data provided by WRC and use riparian buffer width estimates from the CEM riparian survey, summarised for the Waitomo catchment by Kimberley (2019). Existing soil conservation works on hillslopes (including indigenous retirement, protection production plantings, and space-planted trees) were represented using the spatial data supplied by WRC. We also include the stock density data supplied by WRC derived from AgriBase® in the surface erosion sub-model to represent the effect of livestock treading on soil erodibility.

Retro scenario

We include a retrospective scenario ('Retro') to assess the influence of land cover change and erosion mitigations implemented since the mid-1990s. This scenario represented catchment conditions in 1996, corresponding to the earliest land-cover mapping available in LCDB v6.0. All soil conservation works identified in the WRC data set were excluded from the scenario, as they were established after 1996. Areas currently occupied by these mitigation plantings were assumed to have been pasture at that time. Riparian fencing was also removed from the digital stream network (DSN), reflecting pre-mitigation conditions.

---

[12] LCDB v6.0 – Land Cover Database version 6.0, Mainland New Zealand (Manaaki Whenua – Landcare Research, 2025), representing land cover circa 2023. Available at: https://doi.org/10.26060/landcareresearch/LCDBv60.

Future erosion mitigation scenarios

The three mitigation scenarios described below quantified the effect of future erosion mitigations on suspended sediment loads in the upper Waitomo catchment. In each scenario, the mitigations are assumed to be fully implemented and fully matured. Table 2 summarises the areas and length of mitigations.

Mitigation scenario 1 (minimum requirements) (M1):

- Retirement and afforestation: pastoral land on slopes ≥ 35° are retired and transitioned to permanent woody vegetation cover (natives), based on the LiDAR-derived 5 m DEM.
- Space-planted trees: pastoral land on slopes ≥ 26° and < 35° remains in production with implementation of space-planted trees.
- Riparian stock-exclusion fencing: stock-exclusion fencing and setback distances are defined according to the rules described in Regional Plan Change 1 (Waikato Regional Council [WRC] 2020):
    - Regional Plan Change 1 specifies that farmed cattle, horses, deer, and pigs be excluded from water bodies on land with a slope of up to 15°, or on land with slopes greater than 15° where any paddock adjoining the water body has stock units exceeding 18 stock units per grazed hectare at any time.
    - New riparian fencing will be applied to all second-order and higher natural streams, including ‘narrow’ streams as defined under the Sustainable Dairying Water Accord. Fencing along these streams will be set back 3 m from the waterbody edge. No riparian fencing will be applied to first-order streams. For artificial drains wider than 2 m, fencing will be applied with a 1 m setback.

Mitigation scenario 2 (intermediate) (M2):

- Retirement and afforestation: pastoral land on slopes ≥ 30° are retired and transitioned to permanent woody vegetation cover (native), based on the LiDAR-derived 5 m DEM.
- Space-planted trees: pastoral land on slopes ≥ 26° and < 30° remains in production with implementation of space-planted trees.
- Riparian stock-exclusion fencing: stock-exclusion fencing applied to all waterways on slopes ≤ 25°, except 1st order streams, and new fencing will have a 5 m buffer width applied.
- All sinkholes (tomo) retired with a setback of 5 metres.

Mitigation scenario 3 (best case) (M3):

- Retirement and afforestation: pastoral land on slopes ≥ 25° are retired and transitioned to permanent woody vegetation cover (native), based on the LiDAR-derived 5 m DEM. No space-planting.
- Riparian stock-exclusion fencing: stock-exclusion fencing applied to all waterways on slopes ≤ 25°, except 1st order streams, and new fencing will have a 5 m buffer width applied.
- All sinkholes (tomo) retired with a setback of 5 metres.

Table 2. Summary of the area or length of erosion mitigations applied under each scenario in the upper Waitomo catchment

Catchment	Scenario	Retirement and Afforestation (ha)	Space-planted trees (ha)	Riparian stock-exclusion fencing (km, and % of network)
Upper Waitomo	M1	77	255	8 (5%)
	M2	183	149	13 (8%)
	M3	379	-	13 (8%)

Note that scenario M3 does not include space-planted trees (–).

3.3.2 Estimating sediment load reductions from mitigations

Reduction in hillslope erosion from mitigations

The reduction in sediment load from erosion mitigations was represented through changes in land cover associated with each mitigation type. The effectiveness values summarised in Table 3 are provided as an indication of the expected reduction in erosion once a mitigation is fully established, based on published studies. These values are not applied directly as scalar reductions to hillslope erosion loads; rather, they reflect the reduction achieved through the corresponding land-cover change represented in the model. Maturity rates are similarly provided to describe the gradual development of mitigation effectiveness through time, although maturity effects were not explicitly applied in the present study.

Past, present, and future erosion mitigations, and the associated land cover changes, were represented using spatial data supplied by WRC describing the location, type, and year of implementation of soil conservation works within the upper Waitomo catchment. The different soil conservation asset types were matched to the erosion mitigation categories represented in the model (Table 3).

The effectiveness values in Table 3 are derived from published studies and indicate the approximate reduction in erosion associated with each mitigation type once fully established. Conversion to permanent woody cover has a 90% reduction in mass movement erosion based on published data (Pain & Stephens 1990; Phillips et al. 1990; Marden et al 1991; Bergin et al. 1993, 1995; Marden & Rowan 1993; Page et al. 1999; Dymond et al. 2006; Phillips et al 2020). Space-planted trees and gully tree planting are associated with a 70% based on data from Hawley and Dymond (1988), and consistent with Douglas et al. (2009, 2013; McIvor et al. (2015), although the various studies report varying effectiveness (see model limitations). For surface erosion, the reduction from afforestation and bush retirement are represented through changes in the RUSLE cover factor (C: Equation 3) resulting from conversion of pasture to forest or scrub along with changes in the K-factor from removal of livestock grazing and treading. Space-planted trees and gully tree planting do not typically achieve canopy closure and therefore do not reduce surface erosion. Riparian retirement was treated separately through the riparian buffer and bank erosion components of the model, with a reduction of 80% attributable to riparian fencing and stock-exclusion (Dymond et al. 2016; Phillips et al. 2020), although we recognize that published studies report a range of effectiveness values (see discussion in Section 4.4 on model limitations).

Table 3. Summary of maturity and effectiveness of the erosion mitigations on pasture used in the modelling

Erosion mitigation	Years to fully mature	Annual maturity rate[a]	Effectiveness[a]	Soil conservation asset type from WRC data
Conversion to woody cover (afforestation/ bush retirement)	10	10%	90% (mass movement) 50% (surficial)	'Indigenous Retirement', 'Protection Production Plantings'
Space-planted trees	15	6.66%	70% (mass movement)	'Space Planting'
Riparian retirement	2	50%	80% (bank erosion)	'Riparian Retirement', 'Stream Bank Erosion Control Plantings'

[a] Maturity and effectiveness rate derived and summarised from Douglas et al. 2008; Manderson et al. 2011; McIvor et al. 2011; Basher et al. 2018.

Reduction in hillslope sediment delivery to streams from surface erosion

Equation 18 shows the sediment passing factor, the inverse of trapping efficiency, we calculated for the riparian buffer of the jth stream segment (PF_{F_j}) following Zhang et al. (2010):

$$PF_{F_j} = 1 - \frac{k\left(1 - e^{-bw}\right)}{100} \tag{18}$$

where k and b are fitted parameters equal to 90.9 and 0.446, respectively (Zhang et al. 2010), and w is the buffer width. We estimated a mean buffer width for each digital stream segment based on the proportion of land class and the corresponding buffer width intersecting with the segment. The proportion of fenced stream length per segment was derived from existing riparian retirement spatial data provided by WRC. Average riparian buffer width estimates were derived from the CEM riparian survey, summarised for the Waitomo catchment by Kimberley (2019). The trapping relationship was applied at the stream-segment scale using the mean buffer width for each reach, rather than separately for each stream bank based on the mitigation scenario descriptions.

The reduction in sediment load delivered from surface erosion due to fencing and stock-exclusion from riparian retirement in a reach (S_{F_j}) is a function of the proportion of the reach fenced (FR_j) and the buffer passing factor, shown in Equation 19:

$$S_{F_j} = ES_j \times \left(1 - FR_j PF_{F_j}\right) \tag{19}$$

where ES_j is the hillslope load from surface erosion prior to buffer interception for the j^{th} reach per subwatershed.

Reduction in bank erosion

We calculated the reduced sediment load from bank erosion due to fencing and stock-exclusion (B_{F_j}) as shown in Equation 20:

$$B_{F_j} = B_j \times \left(1 - 0.8FR_j\right) \tag{20}$$

where B_j is the net suspended sediment load from bank erosion without the effect of fences reducing erosion. A sediment load reduction of 80% from bank erosion was used for fenced reaches based on previous SedNetNZ applications and published studies of riparian fencing and stock-exclusion (Dymond et al. 2016; Phillips et al. 2020). This reduction reflects the combined effects of reduced stock trampling and foraging on streambanks (Trimble 1994), and the increased bank stability associated with establishment of riparian woody vegetation in the absence of livestock over the longer term. It assumes that sufficient time has elapsed for streambanks to recover and riparian vegetation to become established. Consequently, the 80% reduction should be considered an approximation suitable for catchment-scale modelling rather than a site-specific estimate (see Section 4.4.2).

Riparian fencing estimates and identification of eligible stream reaches

For the contemporary baseline (C2024), we estimated the proportion of stream segments with riparian fencing in the Waitomo catchment using existing riparian retirement spatial data provided by WRC, summarised in Table 4. The fencing data was buffered 10 m and intersected with the DSN to estimate the proportion of each stream segment that was fenced. This 10 m buffer was used to solely to identify stream segments associated with existing fencing and should not be interpreted as the width of the riparian buffer itself. Riparian buffer widths were estimated independently from the CEM riparian survey, summarised for the Waitomo catchment by stream order (Kimberley 2019). The estimated fencing proportions represent the proportion of stream length eligible for fencing that was fenced within each stream-order class. Stream reaches already under woody vegetation were excluded based on LCDB v6.0.

Table 4. Summary of estimated fencing proportions for the digital stream network-based soil conservation and fencing spatial data, and buffer widths based on CEM riparian surveys for the Waitomo catchment, by stream order

Stream order	Farm type	Estimated fencing proportions[a]	Mean buffer width (m)
1	All	35%	5.4
2	All	29%	7.5
3	All	63%	3.4
≥4	All	85%	5.5

[a] The estimated fencing proportions represent the length of stream network that is fenced as a percentage of the total stream length that is eligible for fencing (i.e. excludes reaches under woody vegetation).

Identification of eligible stream reaches for riparian fencing scenarios

Land use associated with each DSN segment was determined using AgriBase® spatial data provided by WRC in combination with LCDB v6.0. These data sets were used to exclude areas unsuitable for riparian fencing (e.g. indigenous forest).

Stream segments classified as ‘Accord streams’ under the Sustainable Dairying Water (Dairy Environment Leadership Group 2013) were identified by transferring classifications previously developed for the REC2 network onto the LiDAR-based DSN using the nearest-segment spatial matching. Accord streams are defined as permanently flowing streams greater than 1 m wide and 30 cm deep and were used to determine riparian fencing eligibility and setback distances under M1. Stream width was estimated from MAF relationships developed for the REC2 network (Booker & Hicks 2013; Semadeni-Davies & Elliott 2016; Whitehead & Booker 2020).

Riparian fencing scenarios

New riparian fencing in Mitigation Scenario 1 (M1) was implemented in accordance with Schedule C of the Proposed Waikato Regional Plan Change 1 (Waikato Regional Council [WRC] 2020). Under this plan, farmed cattle, horses, deer, and pigs must be excluded from water bodies on land with slopes up to 15°, or on steeper slopes (> 15°) where adjoining paddocks have stock unit densities exceeding 18 stock units per grazed hectare at any time.

For the M2 and M3 scenarios, new stock-exclusion fencing was applied to eligible second-order and higher stream segments adjacent to land with slopes ≤ 25. Existing riparian fencing was retained in all scenarios. Slope was derived from the LiDAR-based 5 m DEM and stock-unit density from AgriBase® data provided by WRC. To improve the continuity of low-slope areas and ensure alignment with the DSN, the slope layer was processed using majority filtering, boundary cleaning, and removal of isolated polygons smaller than 400 m² (20 m × 20 m). A 10 m buffer around the DSN was then used to identify stream segments adjacent to eligible low-slope paddock areas.

Slope was derived from the LiDAR-based 5 m DEM and stock-unit density from AgriBase® data supplied by WRC. To improve the continuity of low-slope areas and ensure alignment with the DSN, the slope layer was processed using majority filtering, boundary cleaning, and removal of isolated polygons smaller than 400 m² (20 m × 20 m). A 10 m buffer around the DSN was then used to identify stream segments adjacent to eligible low-slope paddock areas.

Riparian setback distances

New riparian fencing under M1 was implemented in accordance with Schedule C of the Proposed Waikato Regional Plan Change 1 (Waikato Regional Council [WRC] 2020). Second-order and higher stream segments classified as Accord streams were assigned a 3 m setback, while other second-order and higher segments were assigned a 1 m setback. First-order streams were not fenced. For M2 and M3, a uniform 5 m riparian buffer was applied to newly fenced eligible stream segments. Existing riparian buffer widths associated with baseline fencing were retained in all scenarios. Other catchment initiatives may specify alternative setback distances (e.g. 5 m buffers under incentivised management programmes), which were not considered here.

3.4 Reductions for NPS-FM visual clarity attribute bands

To assess the improvement in attribute state under future scenarios, we used the approach developed by Hicks et al. (2019) to estimate the proportional change in mean annual suspended sediment load required to achieve an improved attribute state. This approach is recommended by the Ministry for the Environment in their guidance for implementing the NPS-FM 2020 sediment requirements (Ministry for the Environment 2022), and informed development of the suspended fine sediment attribute for the NPS-FM 2020 (see Hicks & Shankar 2020).

Following Hicks et al. (2019) and Ministry for the Environment (2022), we calculated the proportional change in mean annual suspended sediment load required to achieve a target attribute state as a function of the ratio between the current state visual clarity (visual clarity for each scenario) and the target visual clarity, using Equation 21 at the SOE site:

$$PR_v = 1 - (V_o/V_b)^{1/a} \tag{21}$$

where PR_v is the minimum proportional change in mean annual suspended sediment load required to achieve the target visual clarity, V_o is the target visual clarity for each attribute band (Table 5), and V_b is the current state median visual clarity. We follow the recommendation of the Ministry for the Environment (2022) and assume a in Equation 21 takes the national average reported by Hicks et al. (2019) of -0.76.

We determined the baseline attribute state using the median visual clarity calculated from the most recent 60 visual clarity observations for the Tumutumu SOE monitoring site, provided by WRC (Table 6). Median visual clarity requires monthly observations over a minimum record length of 5 years (60 samples).

To assess the minimum proportional change in suspended sediment load required to improve the attribute band, we used the lower-bound visual clarity for each band (Table 5) for V_o; the upper-bound was used to assess the minimum change in load required for a decline in state from a higher band.

Table 5. Attribute bands and numerical attribute states for suspended fine sediment

Attribute band and description	Numerical attribute state by suspended sediment class (Visual clarity [m])			
	1	2	3	4
A Minimal impact of suspended sediment on instream biota. Ecological communities are similar to those observed in natural reference conditions.	≥1.78	≥0.93	≥2.95	≥1.38
B Low to moderate impact of suspended sediment on instream biota. Abundance of sensitive fish species may be reduced.	<1.78 and ≥1.55	<0.93 and ≥0.76	<2.95 and ≥2.57	<1.38 and ≥1.17
C Moderate to high impact of suspended sediment on instream biota. Sensitive fish species may be lost.	<1.55 and >1.34	<0.76 and >0.61	<2.57 and >2.22	<1.17 and >0.98
National bottom line (NBL)	1.34	0.61	2.22	0.98
D High impact of suspended sediment on instream biota. Ecological communities are significantly altered, and sensitive fish and macroinvertebrate species are lost or at high risk of being lost.	<1.34	<0.61	<2.22	<0.98

(Source: Reproduced from Ministry for the Environment 2020, Table 8.)

The attribute band thresholds for suspended fine sediment are determined by the 'sediment class' associated with each REC2 segment (Table 6). The sediment class of a given segment is determined by the climate, topography, and geological classification (as defined in the REC2) of upstream segments predominantly contributing flow to a given segment. We used the layer denoting suspended sediment class for the REC2 DSN produced by Hicks and Shankar (2020)[13] to identify the sediment class of the segment associated with the SOE monitoring site. This was then mapped onto the stream segment from the LiDAR-based DSN (Figure 4).

[13] Available from the Ministry for the Environment data portal at: https://data.mfe.govt.nz/layer/103687-hydrological-modelling-to-support-proposed-sediment-attribute-impact-testing-2020/

Table 6. Summary details for SOE monitoring site with measured median visual clarity (CLAR, m) derived from black disc measurements

Catchment	Site name	Site ID	REC2 nzsegment ID	Date range used	*n*	Sediment class	Median CLAR	Base state
Upper Waitomo	Waitomo Stm at Tumutumu Rd	1253	3096865	Nov-2019 to May-2025	60	1	0.96	D

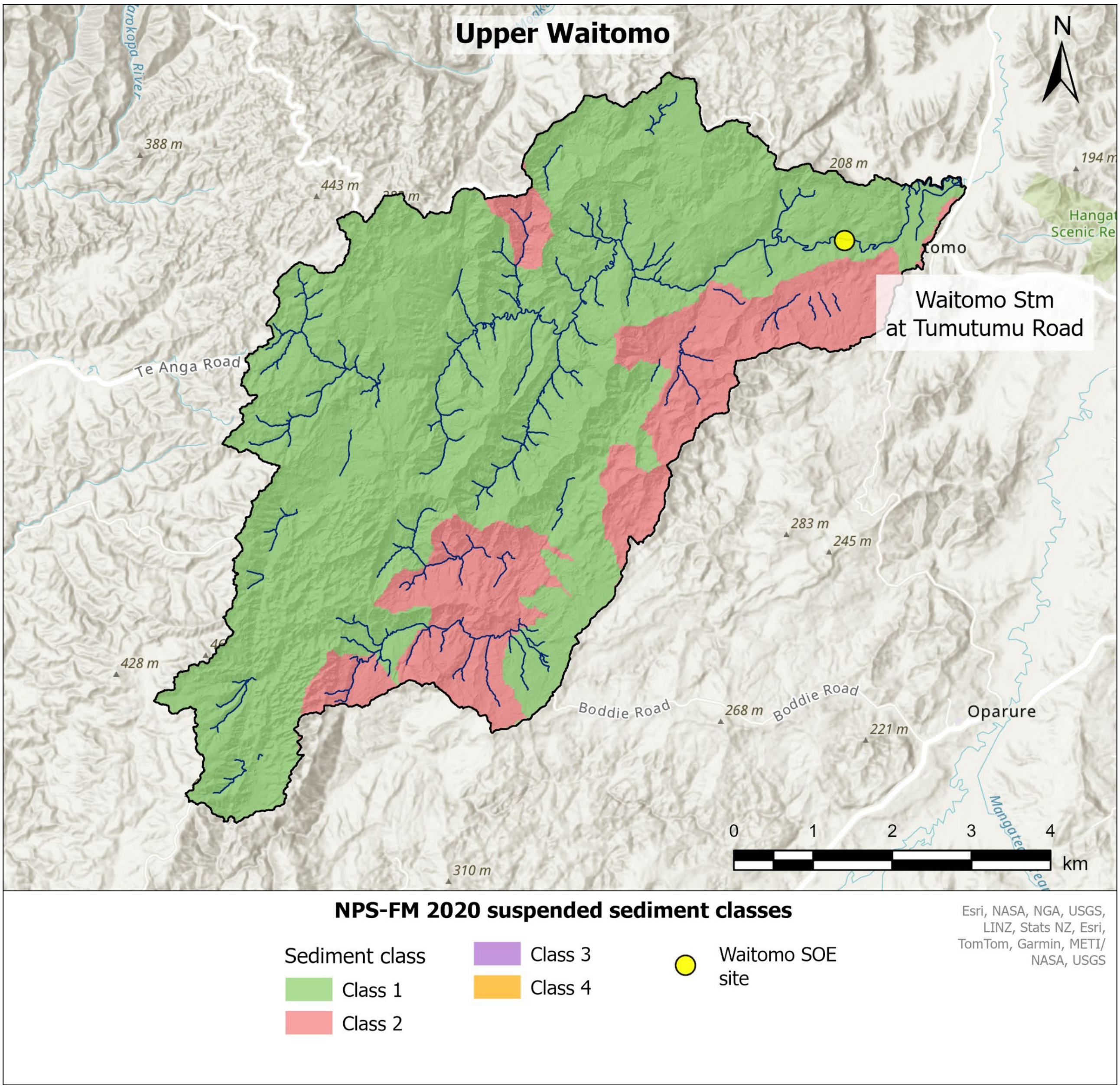

Figure 4. National Policy Statement for Freshwater Management (NPS-FM 2020) suspended sediment classes for the upper Waitomo catchment, and the location of SOE monitoring site.

3.5 Cost-effectiveness of erosion mitigations

Suspended sediment loads were modelled using the LiDAR-based SedNetNZ model for the upper Waitomo catchment. In this study, SedNetNZ was applied to estimate mean annual suspended sediment loads under three mitigation scenarios (Section 3.3.1), comprising bush-retirement or afforestation, space-planted trees, and riparian stock-exclusion fencing. For the purpose of cost-effectiveness analysis, all mitigations were assumed to be fully implemented and mature by 2045, based on an assumed 20-year implementation period agreed with WRC.

3.5.1 Cost estimation of mitigation scenarios

We estimated implementation costs for each mitigation scenario using unit cost estimates provided by WRC (unpublished 2025/26 prices in NZ$). Scenario implementation costs were estimated by multiplying the modelled extent (area) of each mitigation type under the M1–M3 scenarios by the corresponding unit costs presented in Table 7 and summing costs across all mitigation activities. Present values were calculated using discount rates of 2% and 8% to convert future mitigation implementation costs to their equivalent present-day values, reflecting the principle that costs incurred in the future are worth less than the same costs incurred today. All mitigations were assumed to be implemented over a 20-year period and completed by 2045.

Some mitigations required additional fencing costs. For example, native afforestation costs included both establishment costs and retirement fencing of high-slope land, while riparian retirement costs included waterway fencing and riparian planting. The fully loaded costs used in the analysis are summarised in Table 7.

Table 7. Establishment cost (NZ$) of erosion mitigations for the upper Waitomo catchment including WRC-supplied unit costs per mitigation and aggregated costs incorporating associated fencing requirements.

Mitigation	Cost as of 25/26 provided by the WRC[a]	Mitigation	Cost per ha, incorporating estimated fencing [b]
Space-planted trees	$4,730 ha^{-1}	Space-planted trees	$4,730 ha^{-1}
Native afforestation	$7,227 ha^{-1}	Retirement (and fencing)	$13,627 ha^{-1}
Retirement fencing of high slope land/sinkholes	$30-35 m^{-1}		
Riparian planting	$37,774 ha^{-1}	Riparian retirement (and fencing)	$85,903 ha^{-1}
Retirement fencing of waterways (assuming 5 wire-2 electric)[c]	$25 m^{-1}		

[a] Cost data were provided by WRC for each mitigation in the Waitomo catchment and were based on typical planting densities and plant costs. Actual implementation costs will vary depending on site characteristics, existing fencing, terrain, access, contractor rates, and final design.
[b] WRC assumes approximately 1,000 m of fencing per 5 ha of hill country retirement; however, this can vary considerably depending on existing fencing and site configuration.
[c] Riparian retirement was applied to 50% of all new riparian fencing/retirement areas based on WRC guidance. Across the modelled scenarios, the average estimated fencing requirement equates to approximately 2,680 m per hectare of riparian retirement.

3.5.2 Relationships between mitigations and policy-relevant outcomes

Following Polyakov et al. (2024), we derived simplified empirical relationships between erosion mitigation extent and their modelled outcomes to estimate the effectiveness and cost-effectiveness of individual mitigations. Although applied here at a smaller spatial scale, the same analytical framework is appropriate because the objective is to estimate the relative marginal contribution of multiple mitigation measures implemented simultaneously. The framework identifies each measure's marginal effect from cross-sectional variation in where mitigations are placed and in baseline sediment yield, not from the number or size of the modelled scenarios. It is therefore not specific to the regional scale of Polyakov et al. (2024): here the same variation is provided by 969 subwatershed observations, which is sufficient to estimate three coefficients. Since SedNetNZ predicts the combined effects of each mitigation scenario, the regression approach provides a means of decomposing those combined responses into the marginal contribution of individual mitigations, enabling comparison of their relative effectiveness and cost-effectiveness. Here we focus on individual mitigations rather than on the combined scenarios because the policy question is which type of mitigation delivers the largest sediment reduction per dollar, and that ranking cannot be read from scenario totals in which several mitigations are applied together.

The mitigation scenarios were therefore designed to represent realistic catchment management scenarios comprising multiple complementary mitigation measures, rather than experimental scenarios intended to isolate the effect of each mitigation independently. This decomposition does not depend on the small number of scenarios: it is estimated at the subwatershed level across 969 observations (Equation 22, Table 12), where spatial variation in the placement of each mitigation and in baseline sediment yield identifies its marginal effect. The scenarios serve only as the source of that variation, not as the unit of analysis. Running separate mitigation-specific scenarios would have quantified the performance of individual treatments but would not have addressed the objective of estimating the relative marginal contribution of each mitigation within realistic management scenarios. Specifically, we estimated the marginal costs of reducing sediment load at the SOE site at the end of the modelling period (2045).

First, we estimated the relationship between the erosion mitigations and the modelled changes in sediment load. We assumed that mitigations implemented from 2024 to 2045 were related to the changes in sediment load after maturation as in Equation 22:

$$\Delta L_{i,s} = \sum_{k} \beta_k m_{k,i,s} y_i + \varepsilon \qquad (22)$$

where $\Delta L_{i,s}$ is the change in average annual sediment load L (t yr^{-1}) generated by the LiDAR-derived stream segment subwatershed i in a scenario s ; $m_{k,i}$ is the area (ha) of the mitigation measure k implemented in the subwatershed; y_i is the sediment yield (t km^{-2} yr^{-1}) in the subwatershed before the implementation of the works; β_k is the regression parameter to be estimated; and ε is the residual. Like Polyakov et al. (2024), we estimated the model without an intercept.

This regression attributes reductions in sediment load to individual mitigations. However, some works, such as riparian fencing and planting, are typically implemented together and therefore exhibit high correlation, making their independent effects difficult to estimate. To address this, riparian fencing and planting were represented as a single mitigation variable based on the area of riparian retirement. We assumed that the length of riparian fencing was proportional to the retired riparian area. The associated cost estimates reflected this joint interpretation: the costs include planting on 50% of the retired riparian area (based on WRC guidance) and fencing for the equivalent proportional length. Consequently, sediment reductions attributed to riparian retirement represent the combined effects of riparian planting and fencing, and associated costs include both planting and fencing components.

Second, we estimated the relationship between changes in the gross sediment load (i.e. not accounting for the sediment deposition) and the changes in the sediment load at the SOE site (Equation 23):

$$\Delta B_{\ s} = \gamma \sum\nolimits_{i} \Delta L_{i,s} + \varepsilon \tag{23}$$

where $\Delta B_{j,s}$ is the change in sediment load in the catchment j, for scenario s; $\sum_i \Delta L_{i,s}$ is the change in gross annual sediment load L generated by all the subwatersheds i; γ is the regression coefficient to be estimated; and ε is the residual.

This relationship converts the gross sediment reduction, summed across subwatersheds, into the net change delivered to the SOE site, accounting for deposition and storage in transit. It is required because the per-mitigation effects from Equation 22 are estimated on gross subwatershed load and must be carried through to the site to form a cost-effectiveness metric. Because only three scenarios are available, we treat γ as a single calibrated delivery coefficient (Table 13) rather than a statistically estimated relationship, and we place no weight on its standard error.

Third, we estimated changes in visual clarity for each scenario using sediment loads at the beginning (baseline) and at the end of the modelling period. Visual clarity was calculated using Equation (21) and the sediment loads under each scenario at both time points. The difference between baseline and end-of-period visual clarity provides the estimated visual clarity improvement attributable to the mitigation scenario.

The resulting mitigation-level effectiveness and cost-effectiveness metrics should be interpreted as average marginal values derived from the suite of modelled scenarios rather than precise estimates of the independent effect of each mitigation measure in isolation. Direct comparison of modelled scenarios provides information on the overall effectiveness and cost-effectiveness of the mitigation packages (M1–M3), whereas the regression approach provides an indicative comparison of the relative marginal contribution and cost-effectiveness of the individual mitigation measures comprising those packages. The package-level conclusions come from the directly modelled scenario-level metrics, while the mitigation-level estimates are used as an indicative ranking of the relative cost-effectiveness of individual measures rather than as standalone treatment effects.

3.5.3 Cost-effectiveness

We modelled the cost (in New Zealand dollars, NZ$) of mitigations as the sum of establishment costs discounted to present value. Unlike Polyakov et al. (2024), we do not include opportunity cost, carbon benefits, or ongoing maintenance costs. We calculated the Present Value of Costs (PVC) for each mitigation over the implementation period (from 2024 to 2045).

For each subwatershed i, mitigations were assumed to be implemented progressively over a 20-year period from 2024 – 2045, inclusive. The costs were calculated annually and discounted to 2024 using a chosen discount rate (*r*), as shown in Equation 24.

$$PVC_{i,k} \ = \sum_{t=2024}^{2045} \frac{C_{est,i,t}}{(1+r)^{t-2024}} \tag{24}$$

Where $PVC_{i,k}$ is the present value cost of mitigations k *in subwatershed* i, $C_{est,i,t}$ are establishment costs, r is the discount rate and t is a year.

Annual establishment costs ($C_{est,i,t}$) were assumed to occur in the year a mitigation is implemented. Since we assume that implementation is gradual, the annual cost is given by Equation 25 as:

$$C_{est,i,t} = \frac{c_k \times m_{i,k}}{20} \tag{25}$$

where c_k is the cost of the mitigation k (Table 7), $m_{i,k}$ is the area of the mitigation k in the subwatershed i, and 20 is the number of years over which works are implemented.

Discount rates of 2% and 8% were used to convert future implementation costs to their equivalent present-day values, reflecting the time value of money. These rates were selected to evaluate the sensitivity of cost-effectiveness estimates to different assumptions regarding future costs.

To estimate cost-effectiveness, mitigation costs were combined with the effectiveness relationships described above. After obtaining the PVC (Equation 24) and estimating the relationships via regression models (Equations 22 & 23), we derived several policy-relevant cost-effectiveness metrics for each type of mitigation.

First, we calculated the physical effectiveness of mitigations as the reduction in suspended sediment load per unit area of mitigation implemented (t yr^{-1} ha^{-1}). Second, we estimated the marginal cost of reducing sediment loads at the SOE monitoring site using discounted establishment costs for both 2% (base case) and 8% (high rate), using Equation 26:

$$MCSL_{i,k} = PVC_{i,k}/(y_i \beta_k \gamma_j) \tag{26}$$

where $MCSL_{i,k}$ is the marginal cost of reducing sediment load (NZ\$ t^{-1} yr^{-1}) at the SOE site by applying mitigation work k in subwatershed i; $PVC_{i,k}$ is the present value of mitigations k; y_i is the sediment yield in the subwatershed i; and β_k and γ_j are the regression coefficients.

To relate sediment reductions to water-quality outcomes, we used the established nonlinear relationship between sediment load and visual clarity (Equation 21). Changes in visual clarity (m) at the SOE monitoring site were estimated from the predicted reductions in net sediment load. Using this relationship, we estimated the marginal cost of improving visual clarity, expressed in millions of NZ$ per m increase in visual clarity ($ million m^{-1}), under both discount rates. Results were summarised across subwatersheds using area-weighted statistics.

In addition to the regression-derived mitigation-level cost-effectiveness metrics, overall scenario-level cost-effectiveness was calculated by dividing the total implementation cost of each mitigation scenario by the corresponding reduction in mean annual net suspended sediment load at the SOE site. These scenario-level metrics provide a direct comparison of the overall performance of the modelled mitigation packages and complement the mitigation-level estimates by assessing the cost-effectiveness of the combined mitigation scenarios.

4 Results and discussion

4.1 LiDAR-based SedNetNZ erosion and sediment load model for the upper Waitomo catchment

This section provides an overview of the outputs from the upgraded shallow landslide, surface and riverbank erosion sub-models under contemporary baseline (C2024) conditions, then considers the catchment suspended sediment budgets for both the contemporary baseline and future mitigation scenarios. The upper Waitomo catchment layers associated with the LiDAR-based version of SedNetNZ that accompany the present report are summarised in Table A1.1 of Appendix 1.

4.1.1 Shallow landslide erosion

Shallow landslide erosion may be expressed as the mean annual sediment yield from shallow landslides delivered to the stream network. This representation of shallow landslide erosion does not imply landslide erosion occurs every year. Instead, it takes the average – on an annual basis – of the sediment load generated by discrete landslide-triggering events estimated to occur over multi-decadal intervals. This approach allows for the construction of sediment budgets where the contributions from each erosion process may be expressed in the same units: either as suspended sediment loads (t yr^{-1}) or net sediment yields (t km^{-2} yr^{-1}).

Figure 5 shows the spatial patterns in modelled mean annual net sediment yields (per pixel) from shallow landslides for the upper Waitomo catchment. These pixel-based yields form the basis for computing the shallow landslide sediment load contribution for each subwatershed in the DSN. The highest net sediment yields (> 750 t km^{-2} yr^{-1}) from shallow landslide erosion occurred most extensively on the pastoral hill country, particularly in the upper areas of the catchment. In contrast, the forested and lower sloped terrain had significantly lower net sediment yields (< 25 t km^{-2} yr^{-1}) from landslide erosion, which reflects the lower susceptibility of this terrain to the occurrence of landslides (Figure 5).

The mean annual net sediment load delivered to the stream network from shallow landslide erosion amounted to 4.1 kt yr^{-1} for the upper Waitomo catchment, using the upgraded shallow landslide sub-model with the LiDAR-derived DEM.

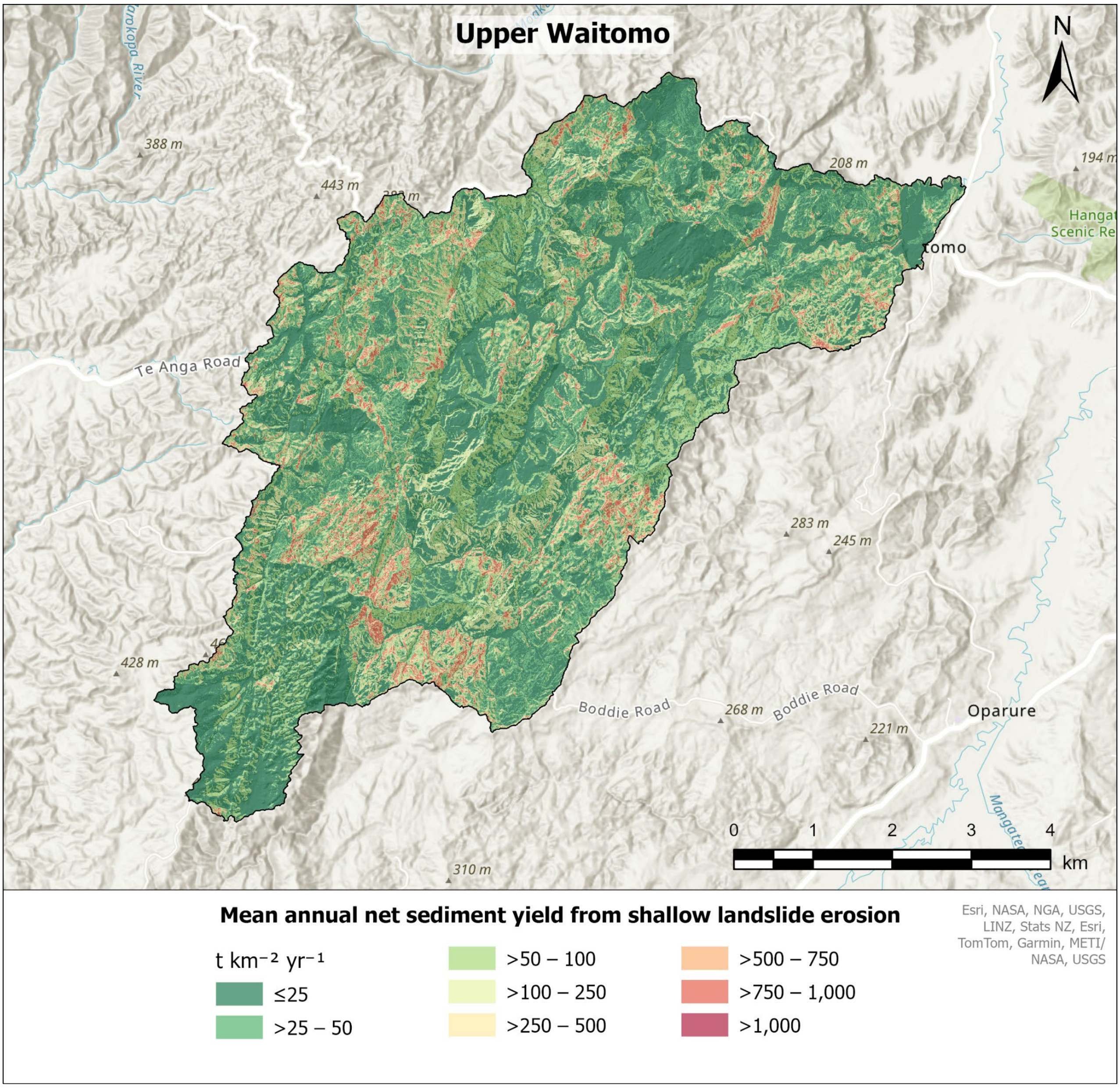

Figure 5. Mean annual net sediment yield (t km^{-2} yr^{-1}) from shallow landslide erosion delivered to the upper Waitomo stream network based on 2023 land cover from LCDB v6.0 and existing soil conservation works, displayed over the underlying hillshade layer.

4.1.2 Surface erosion

Figure 6 shows the modelled mean annual net sediment yields from surface erosion (sheet and rill erosion) delivered to the upper Waitomo stream network. The spatial pattern in surface erosion reflects the spatial variations in the RUSLE factors. Higher rainfall erosivity tended to occur over elevated terrain due to orographic effects that produce higher rainfall. Soil erodibility increases where surface soils have lower organic matter and higher silt content. Steep and convergent terrain concentrates surface run-off that may increase erosion, while vegetation cover has a critical role in protecting the soil surface from raindrop impact and increasing surface roughness that reduces overland flow velocities.

The highest surface erosion rates (>1,000 t km^{-2} yr^{-1}) tend to occur in hilly areas with higher rainfall and steep, convergent terrain (Figure 6), notably in the north-western areas of the catchment. Within these areas, those locations lacking vegetation cover or where soils tend to have higher silt content exhibited higher surface erosion rates. The mean annual net sediment load delivered to the stream network from surface erosion amounted to 2.4 kt yr^{-1} in the upper Waitomo catchment, using the RUSLE sub-model with the LiDAR-derived DEM.

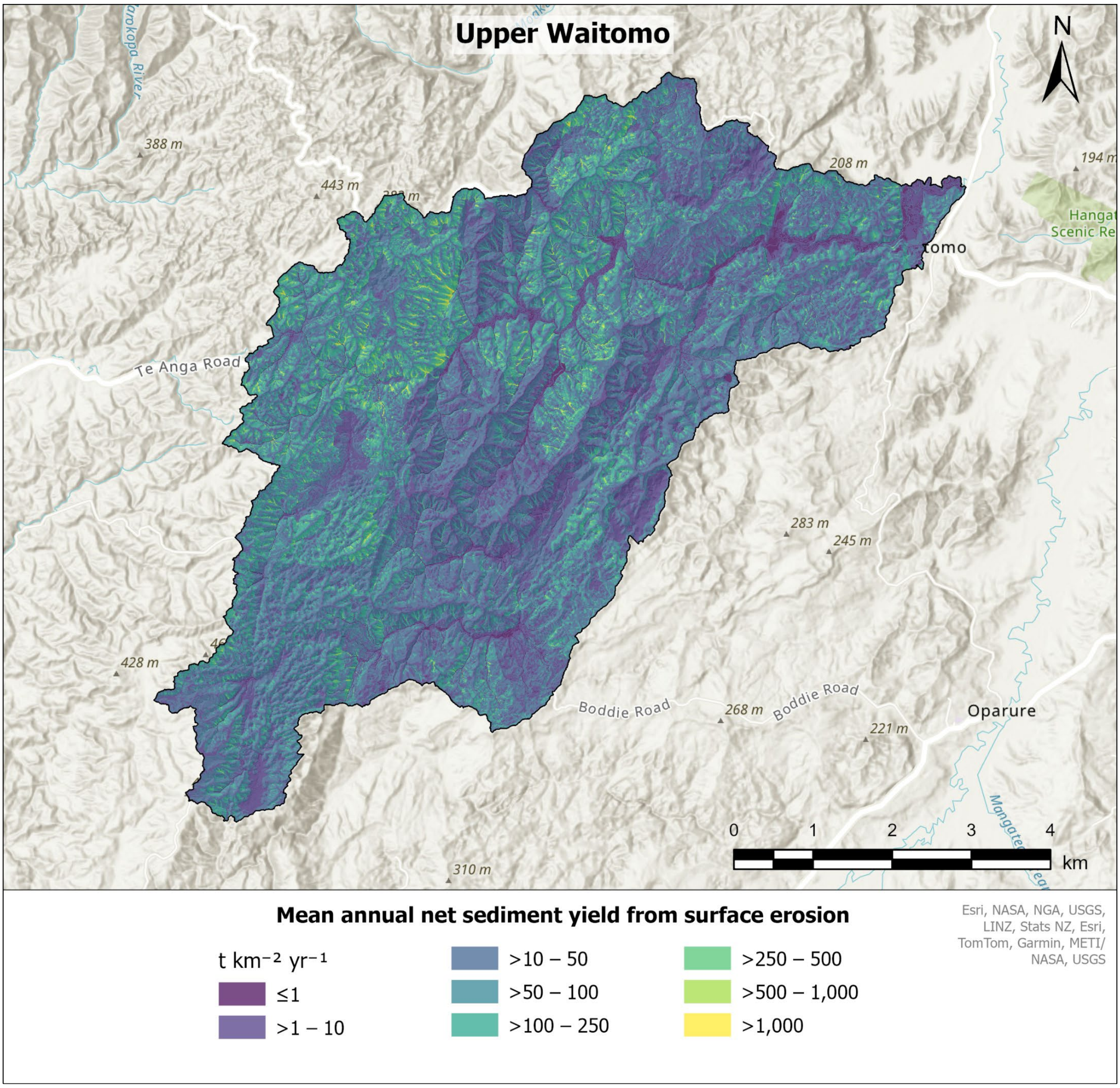

Figure 6. Mean annual net sediment yield (t km^{-2} yr^{-1}) from surface erosion delivered to the upper Waitomo stream network based on 2023 land cover from LCDB v6.0 and existing soil conservation works, displayed over the underlying hillshade layer. The sediment yields account for sediment trapping by riparian buffers, which is determined for each subwatershed and applied across all pixels within the subwatershed.

4.1.3 Riverbank erosion

The modelled mean annual net sediment load from bank erosion equated to 0.26 kt yr^{-1} for the upper Waitomo. This total net load compares with 0.17 kt yr^{-1}, based on the previous region wide SedNetNZ estimates from Vale & Smith (2024). Most of this increase in sediment load contribution from bank erosion was attributable to the increase in the length of the DSN (Figure 2). This increase in network length largely reflects the improved representation of channel sinuosity based on the LiDAR-derived DEM as well as the difference in channel initiation threshold compared to the REC2 digital network (Figure 2). The overall increase was less than that observed in the CEM catchments (cf. Vale et al. 2025a,b), owing to numerous watersheds lacking defined surface drainage due to the karst landscape. Figure 7 shows the spatial pattern in predicted reach-averaged mean annual net suspended sediment yields from bank erosion for upper Waitomo catchment.

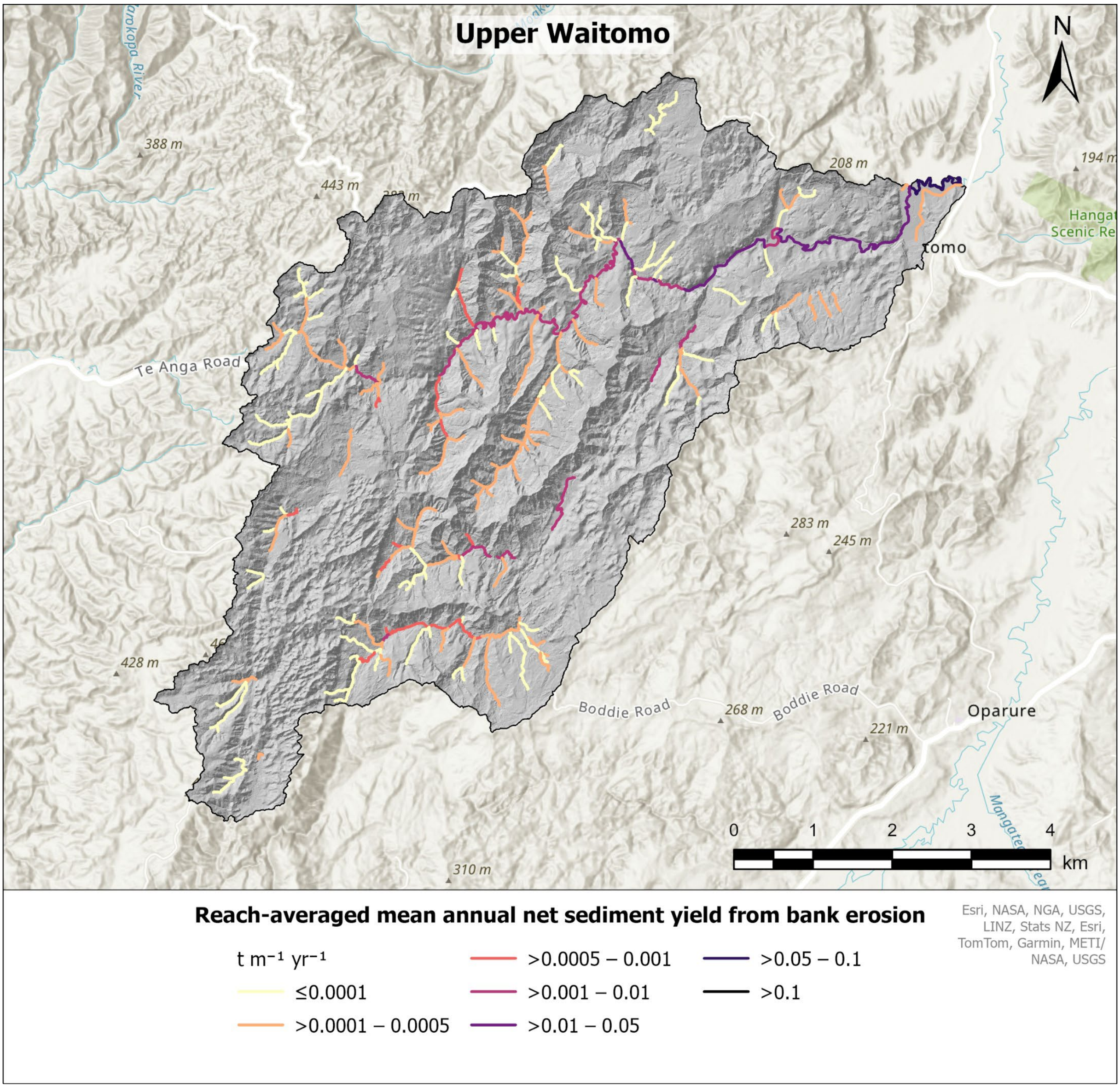

Figure 7. Predicted reach-averaged mean annual net bank sediment yield (t m^{-1} yr^{-1}) per stream segment length for each segment for the LiDAR DEM-derived digital stream network in the upper Waitomo catchment.

4.1.4 Catchment suspended sediment budgets

Contemporary baseline (C2024) and retrospective (Retro) scenarios

Table 8 summarises the modelled mean annual erosion loads, and net suspended sediment load delivered to the catchment outlet, as well as the erosion process contributions to suspended sediment loads in the LiDAR-based SedNetNZ sediment budgets for the upper Waitomo catchment.

Figure 8 shows the mean annual net suspended sediment load per subwatershed, which is the load that accumulates downstream while accounting for losses of sediment into long-term storage in lakes and on floodplains. The net suspended sediment load delivered to the catchment outlet amounted to 5.7 kt yr^{-1} for the upper Waitomo catchment. Over a multi-decadal timescale, shallow landslides contribute an estimated 61% of the suspended sediment load. Surface erosion accounts for 36% and riverbank erosion contributes 4%.

Figure 9 shows the spatial pattern in mean annual net sediment yields (t km^{-2} yr^{-1}) per subwatershed for the upper Waitomo catchment. The sediment yield was calculated as the sum of net sediment loads from each erosion process present within each subwatershed divided by the subwatershed area. This does not account for downstream storage of sediment in lakes and on floodplains. The largest sediment yields typically occurred in areas of pastoral hill country on erodible, soft rock terrain as well as along sections of eroding river channel. Lower sediment yields occurred in areas with woody vegetation cover or low slope. In a few cases, high yields (t km^{-2} yr^{-1}) occurred in subwatersheds with relatively low total erosion loads (t yr^{-1}) due to the very small areas of these subwatersheds (< 0.005 km^2).

Under the retrospective (Retro) scenario where erosion mitigations (soil conservation works) were removed, the net suspended sediment load delivered to the catchment outlet amounted to 8.5 kt yr^{-1} for the upper Waitomo catchment. Over a multi-decadal timescale, the relative erosion process contribution was similar to the contemporary estimates, with shallow landslides contributing an estimated 63% of the suspended sediment load. Surface erosion accounted for 31% and riverbank erosion contributed 6%.

Table 8. Summary of mean annual erosion load, mean annual net sediment load, and erosion process load contribution estimated for the contemporary baseline (C2024) and retrospective ('Retro') scenario for the upper Waitomo catchment using the LiDAR-based SedNetNZ model

Catchment	Scenario	Erosion load[a] delivered to the stream network (kt yr^{-1})	Mean annual net sediment load delivered to the catchment outlet (kt yr^{-1})	Erosion load delivered to the stream network from each process [a] (kt yr^{-1}, %)		
				Shallow landslide erosion	Surface erosion	Riverbank erosion
Upper Waitomo	C2024	6.8	5.7	4.1 61%	2.4 36%	0.26 4%
	Retro	9.8	8.5	6.2 63%	3.0 31%	0.56 6%

[a] Erosion load refers to the mean annual sediment load delivered to a stream segment from the erosion processes occurring in a subwatershed.

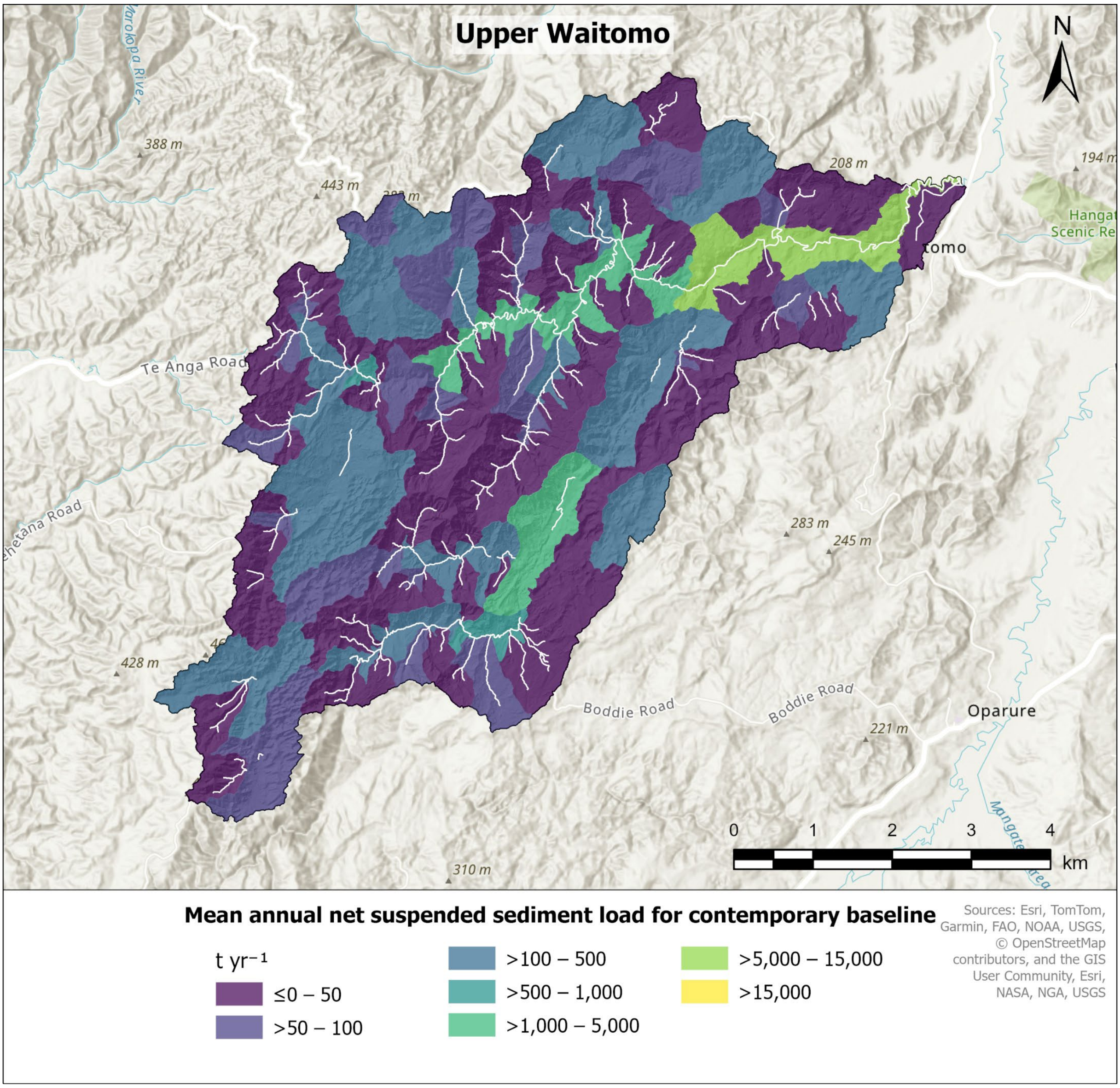

Figure 8. Mean annual net suspended sediment load (t yr^{-1}) accumulated downstream for the contemporary baseline (C2024) based on 2023 land cover from LCDB v6.0 and existing soil conservation works displayed for subwatersheds over the underlying hillshade layer and showing the digital stream network (white).

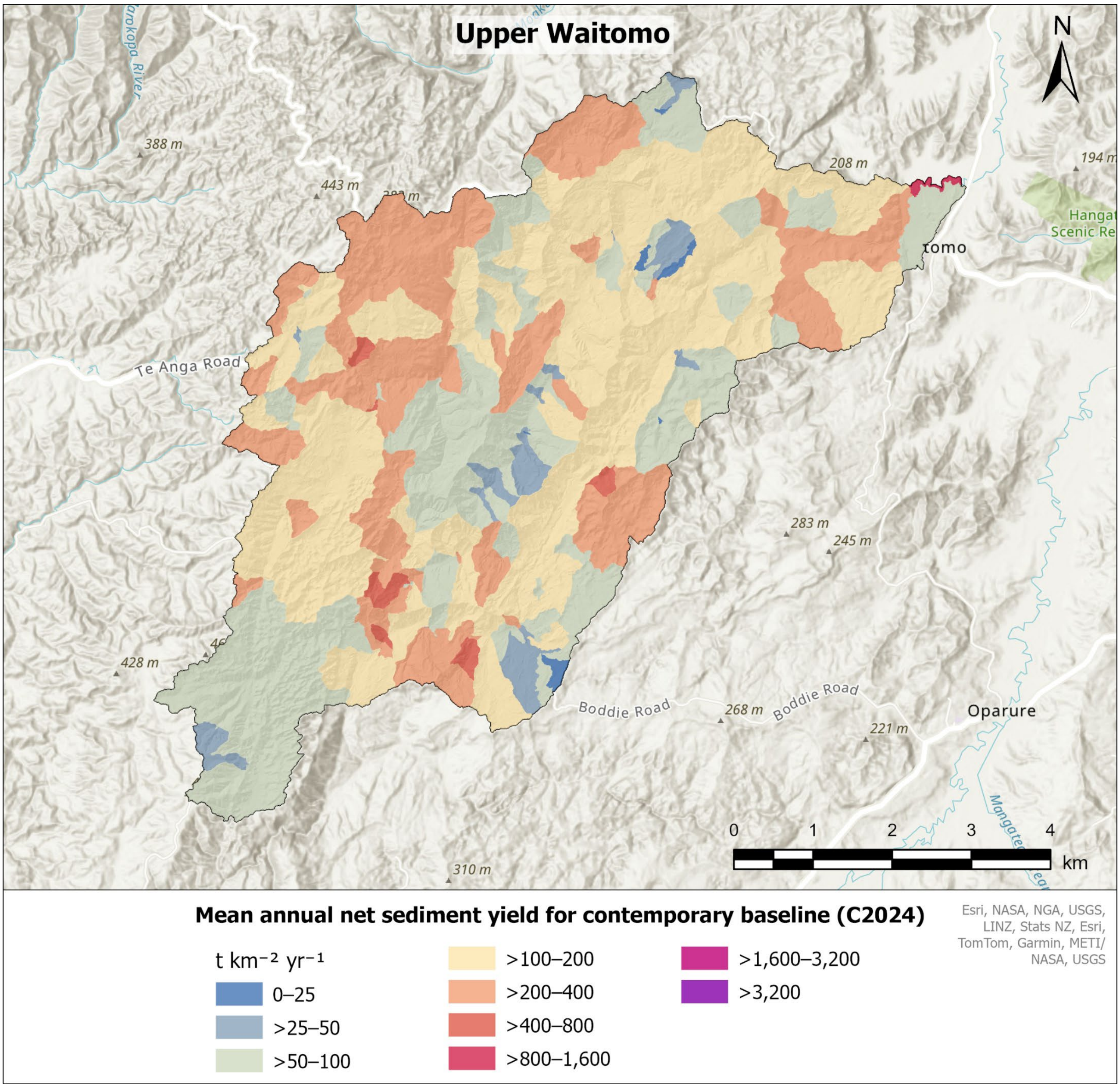

Figure 9. Mean annual net sediment yield (t km^{-2} y^{-1}) per subwatershed and displayed by sediment-yield class for the 2024 contemporary baseline (C2024) based on 2023 land cover from LCDB v6.0 and existing soil conservation works displayed over the underlying hillshade layer.

Future mitigation scenarios

Table 9 presents erosion loads for the future mitigation scenarios, while mean annual net sediment yields (t km^{-2} yr^{-1}) are shown in Figure 10 for the full implementation of the M1 scenario. Figure 11 shows the reductions in mean annual net sediment yield for the future mitigation scenarios relative to contemporary baseline.

Under the M1 scenario, total erosion load decreased by 24% relative to the contemporary baseline – to 5.2 kt yr^{-1}. Larger reductions of 36% and 45% were observed under the M2 and M3 scenarios, resulting in total erosion loads of 4.9 and 4.6 kt yr^{-1} (Table 9). The progressively larger reductions reflect the increasing extent of mitigation applied under each scenario, particularly the expansion of retirement and space-planted trees onto a greater area of erosion-prone hill country, with mitigation primarily targeted to subwatersheds with the highest baseline erosion rates. The largest reductions occurred in the western part of the catchment, where steep terrain, high baseline erosion rates, and greater concentrations of mitigations resulted in larger decreases in sediment yield relative to the contemporary baseline.

Table 9. Erosion loads (kt yr^{-1}) for the upper Waitomo catchment modelled under future erosion mitigation scenarios M1–M3

Catchment (C2024: kt yr^{-1})	Scenario	Erosion load[a] delivered to the stream network (kt yr^{-1})	Mean annual net sediment load delivered to the catchment outlet (kt yr^{-1})	Difference from contemporary baseline (C2024) (kt yr^{-1}, %)	
				Erosion load delivered to the stream network	Mean annual net sediment load delivered to end of catchment
Upper Waitomo (6.8)	M1	5.2	4.3	−1.6 −24%	−1.3 −24%
	M2	4.9	4.1	−1.9 −36%	−1.5 −27%
	M3	4.6	3.8	−2.2 −45%	−1.8 −32%

[a] Erosion load refers to the mean annual sediment load delivered to a stream segment from the erosion processes occurring in a subwatershed.

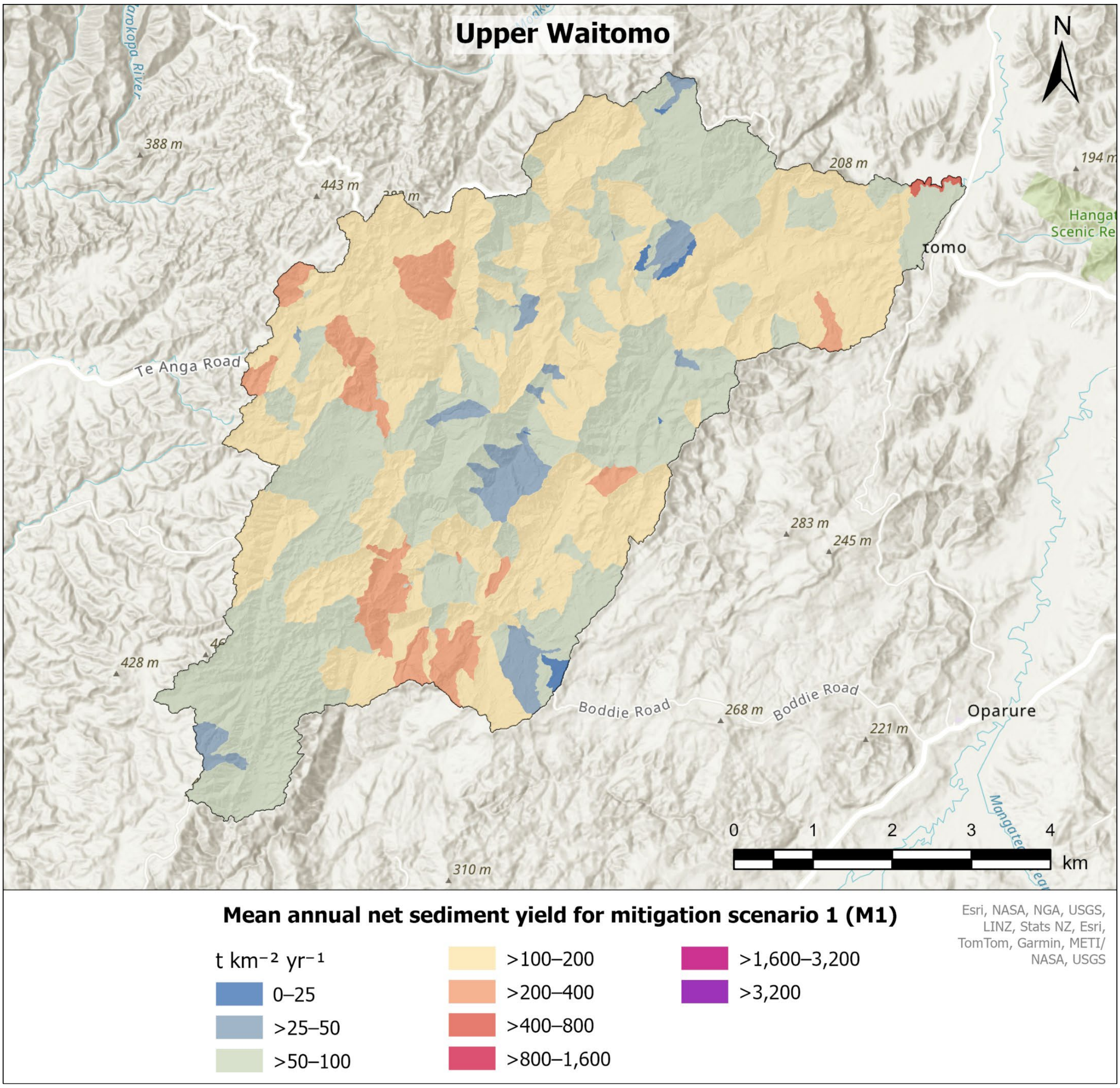

Figure 10. Mean annual net sediment yield (t km^{-2} y^{-1}) per subwatershed and displayed by sediment-yield class for full implementation of the M1 scenario using the LiDAR-based digital stream network displayed over the underlying hillshade layer.

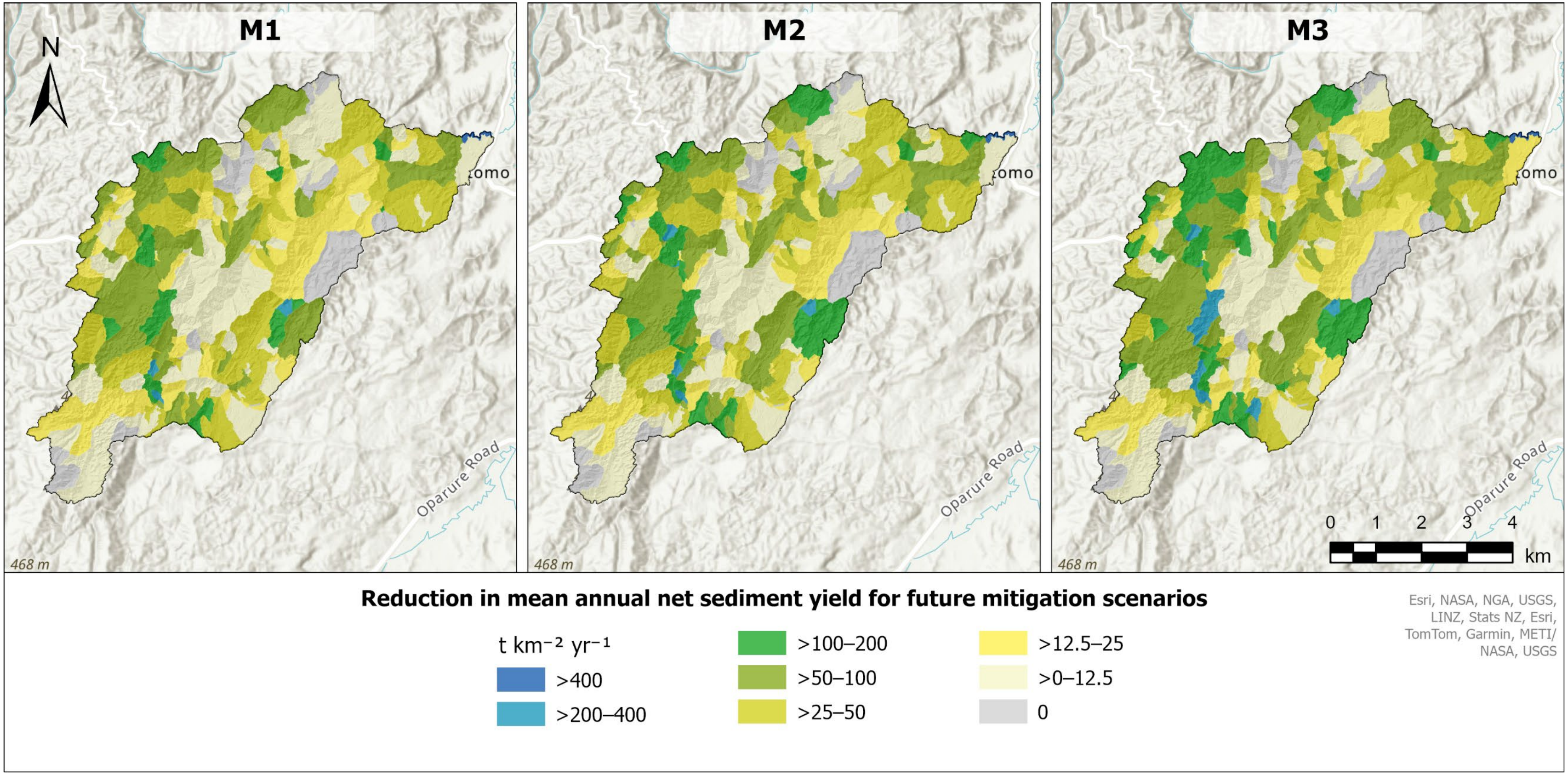

Figure 11. Reduction in mean annual net sediment yield (t km^{-2} yr^{-1}) for the upper Waitomo catchment relative to the 2024 contemporary baseline (C2024) modelled for the M1, M2 and M3 erosion mitigation scenarios.

4.2 Sediment load reductions required to meet NPS-FM visual clarity attribute bands

We modelled suspended sediment load reductions required to meet the NPS-FM 2020 suspended fine sediment attribute bands for the ‘Waitomo Stream at Tumutumu Road’ SOE site in the upper Waitomo catchment. Our modelling assessed proportional reductions needed under both the contemporary baseline (C2024) and future mitigation scenarios.

We determined the baseline attribute state for the Tumutumu SOE monitoring site using the median measured visual clarity based on data provided by WRC (see Section 3.4). Table 10 shows the proportional reductions (%) in suspended sediment load required to achieve the NPS-FM attribute bands and the NBL at the SOE site for the contemporary baseline and future mitigation scenarios.

The Tumutumu SOE monitoring site currently has a D attribute band base state and requires a 36% reduction in sediment load to achieve the NBL for the contemporary baseline. Achieving the B and A attribute bands would require load reductions of 47% and 56%, respectively (Table 10).

Under the mitigation scenarios, progressively smaller reductions in suspended sediment load are required to achieve the NBL and attribute bands relative to the contemporary baseline. Under M1, the reduction required to achieve the NBL decreases from 36% to 17%, with further mitigation under M2 reducing this to 13%, and under M3 to 6%. A similar pattern is observed for the reductions required to achieve the B and A attribute bands, which decrease from 47% and 56% under the baseline to 22% and 35%, respectively, under M3. These improvements reflect the increasing extent of erosion mitigation applied under the scenarios, particularly retirement, afforestation, space-planted trees, and riparian management on erosion-prone land upstream of the SOE site. However, none of the scenarios fully achieve the NBL or visual clarity attribute targets, indicating that additional mitigation would still be required to meet the NPS-FM objectives.

Table 10. Proportional reductions (%) in suspended sediment load still required to achieve National Policy Statement for Freshwater Management (NPS-FM 2020) attribute bands (C, B or A) and the NBL at the ‘Waitomo Stream at Tumutumu Road’ SOE monitoring site for contemporary baseline and mitigation scenarios (M1, M2 and M3)

Site name	Scenario	Proportional reductions (%) in load required		
		C (NBL) %	B %	A %
Waitomo Stm at Tumutumu Rd Site ID: 1253 Base Attribute State: D	Contemporary baseline (C2024)	36%	47%	56%
	Mitigation scenario 1 (M1)	17%	31%	43%
	Mitigation scenario 2 (M2)	13%	28%	40%
	Mitigation scenario 3 (M3)	6%	22%	35%

4.3 Cost-effectiveness of erosion mitigations

4.3.1 Cost estimation of mitigation scenarios

Table 11 summarises the extent of mitigations and the resulting total implementation costs for each scenario. Total costs increased substantially across scenarios, reflecting the greater area of afforestation and riparian retirement. Scenario M1 had the lowest total cost, while M3 was the most expensive primarily due to the large afforestation area. Because implementation costs are assumed to occur over 20 years, discounted totals at 2% and 8% were lower than undiscounted values. Overall, the scenarios spanned a wide cost range, providing a useful basis for comparison.

Table 11. Extent of mitigations and total establishment costs (NZ$) for each scenario; PV– Present Value

Scenario	Mitigations				Total establishment costs		
	Riparian Fencing (m)	Riparian area (ha)	Space-planted trees (ha)	Afforestation (ha)	Total cost, undiscounted ($m)	PV @2% ($m)	PV @8% ($m)
M1	7,646	2.0	255	77	2.5	2.0	1.6
M2	12,853	5.2	149	183	3.6	3.0	2.3
M3	12,840	5.2	-	379	5.6	4.6	3.5

4.3.2 Relationships between mitigations and policy-relevant outcomes

We developed models (Equation 22) and (Equation 23) using outputs from the LiDAR-based version of SedNetNZ from three scenarios (M1, M2, and M3). Like Polyakov et al. 2024, our model was estimated without an intercept to attribute all effects to the mitigations. Table 12 presents the results of estimating the relationship between erosion mitigations and modelled changes in sediment load (Equation 22). The coefficients are statistically significant and provide a basis for comparing the relative effectiveness of mitigations.

Table 12. Regression results (and standard errors) of the relationship between the erosion mitigations and changes in suspended sediment load at the subwatershed level

Variable	Dependent variable: change in sediment load
Area of afforestation (ha) × yield	0.024*** (0.000)
Area of space-planted trees (ha) × yield	0.020*** (0.001)
Area of riparian exclusion (ha) × yield	0.048*** (0.003)
Number of observations	**969**
R^2	**0.863**

Significance levels: * $p < 0.1$, ** $p < 0.05$, *** $p < 0.01$.

Table 13 presents the results of estimating the relationship between changes in the gross sediment load and changes in the sediment load at the SOE site (Equation 23).

Table 13. Regression results (and standard errors) from the relationship between the changes in gross and net sediment load at the SOE site at the catchment level

Variable	Dependent variable: change in sediment load the SOE site
Change in gross sediment load	0.837***
	(0.002)
Number of observations	**3**
R^2	**1.000**

Notes: Significance levels: * $p < 0.1$, ** $p < 0.05$, *** $p < 0.01$. With only three observations, this regression should be treated as calibration and not as a statistically estimated relationship. The R^2 of 1.000 is a mechanical consequence of fitting a single slope through three points.

With only three observations, we treat the gross-to-net relationship as a scaling factor that converts catchment-wide sediment reductions to the change at the SOE site, not as a statistically estimated model, and we do not interpret its R^2 or standard error. The coefficient (γ) enters the cost-effectiveness calculation as the conversion from gross to net reduction at the site (Equation 26).

4.3.3 Cost-effectiveness

We report both the overall cost-effectiveness of the modelled mitigation scenarios and the cost-effectiveness of individual mitigations. Scenario-level metrics provide a direct comparison of the overall performance of the mitigation packages (M1–M3), while mitigation-level cost-effectiveness informs the prioritisation and combination of individual mitigation measures. The regression analysis uses spatial variation in the mitigation extents and locations across scenarios M1–M3 to estimate the marginal effects of individual mitigation measures.

The two sets of metrics are constructed differently and answer different questions, so they are not expected to reconcile arithmetically. The scenario-level metric is an average: the total establishment cost of a package divided by its total net reduction in mean annual suspended sediment load at the SOE site, taken directly from the SedNetNZ output. The mitigation-level metric is marginal: a regression-derived, area-weighted cost per tonne for each measure, estimated from spatial variation across subwatersheds. The scenario metric answers what a given package costs per tonne delivered; the mitigation metric answers which measure reduces the most sediment per dollar. We use the scenario-level results as the primary basis for comparing packages, and the mitigation-level results as an indicative ranking of the relative cost-effectiveness of the individual measures within them.

Scenario-level cost-effectiveness

Table 14 summarises the overall cost-effectiveness of the three modelled mitigation scenarios, calculated by relating total establishment costs to the corresponding reduction in mean annual suspended sediment load at the SOE site. These scenario-level metrics provide a direct comparison of the overall performance of the mitigation packages and complement the regression-derived mitigation-level results presented below.

Table 14. Overall cost-effectiveness of the modelled mitigation scenarios based on reductions in mean annual net suspended sediment load (from Table 9) and total establishment costs (from Table 11)

Scenario	Net sediment-load reduction (t yr^{-1})	Undiscounted cost per unit reduction (\$ t^{-1} yr)	PV @ 2% (\$ t^{-1} yr)	PV @ 8% (\$ t^{-1} yr)
M1	1,300	1,920	1,540	1,230
M2	1,500	2,400	2,000	1,530
M3	1,800	3,110	2,560	1,940

At the scenario level, M1 provided the lowest cost per unit reduction in suspended sediment load, followed by M2 and then M3 (Table 14). This ranking is consistent with the composition of each package and with the mitigation-level results presented below. M1 is dominated by space-planted trees, which the regression analysis identifies as the most cost-effective measure per tonne of sediment reduced. M3, by contrast, consists almost entirely of afforestation and contains no space planting, and afforestation carries a higher marginal cost per tonne. The scenario-level cost for M1, \$1,540 t^{-1} yr^{-1} (PV @ 2%), falls between the mean marginal cost of space-planted trees (about \$1,190 t^{-1} yr^{-1}) and that of afforestation (about \$2,690 t^{-1} yr^{-1}), reflecting its mix of the two measures. The two analyses therefore point in the same direction: the directly modelled scenario metric and the regression-derived component metric each rank the cheaper packages and the cheaper measures consistently, which provides mutual support for both sets of estimates.

Mitigation-level cost-effectiveness

The regression-derived mitigation-level effectiveness and cost-effectiveness metrics are presented in Table 15. The marginal cost of reducing suspended sediment loads and improving visual clarity at the SOE site depends on the cost per unit area of mitigations, the effectiveness of those works, and sediment yields within stream segment subwatersheds. These factors vary considerably across the catchment. To illustrate the spatial variation in effectiveness and cost-effectiveness, the analysis focuses on mitigable areas of the catchment. All effectiveness and cost-effectiveness statistics in Table 15 are computed across the subwatersheds in which each mitigation occurs, separately within each scenario, and weighted by the area of that mitigation. A range quoted across scenarios is the spread of the per-scenario means, whereas percentiles (for example, under M2) describe the distribution across subwatersheds within that scenario.

Costs represent annualised establishment and fencing costs, assuming mitigations are implemented gradually between 2024 and 2045 (see Section 3.5.2). A 2% discount rate was used as the base rate, with an 8% rate used for sensitivity analysis (New Zealand Treasury, 2024). The analysis includes only subwatersheds where mitigations occur under scenarios M1, M2, and M3 (Table 2). The area of mitigation in each subwatershed was used as a weighting factor when calculating distributions. Here we report mean values and distributions (standard deviation, quartiles, medians, and 5th and 95th percentiles) for mitigation effectiveness (t yr^{-1} ha^{-1}) and cost-effectiveness metrics, including the marginal cost of reducing sediment load (\$ t^{-1} yr^{-1}) and the marginal cost of improving visual clarity (\$ million m^{-1}) at both discount rates (Table 15).

Panel A (Table 15) summarises the effectiveness of mitigations across scenarios and mitigation types. Effectiveness is defined as the average reduction in annual suspended sediment load achieved per hectare of mitigation.

- Riparian retirement delivers the highest average effectiveness, reducing sediment loads by approximately 6.1–7.5 t yr^{-1} ha^{-1} across scenarios, although variability is substantial (CV =

0.59–0.61), reflecting heterogeneous site conditions. Afforestation achieves moderate reductions of 4.6–4.9 t yr^{-1} ha^{-1} with lower relative variation (CV = 0.41). Space-planted trees produce the lowest average reductions (3.8 t yr^{-1} ha^{-1}) with similar variability to afforestation. The statistics indicate considerable spatial variability within mitigation types. For example, under M2, riparian retirement ranges from 3.5 t yr^{-1} ha^{-1} at the 5th percentile to 17.6 t yr^{-1} ha^{-1} at the 95th percentile. This variability primarily reflects differences in baseline sediment yields, erosion processes, and the location of mitigations within the catchment, with mitigation applied in higher-yielding areas producing greater sediment reductions per unit area.

The regression-derived mitigation-level cost-effectiveness, expressed as the marginal cost of reducing sediment load (\$ t^{-1} yr^{-1}), is presented in Panels B (2% discount rate) and C (8% discount rate).

- At a 2% discount rate, space-planted trees appeared the most cost-effective option, with average marginal costs of \$1,190–1,210 t^{-1} yr^{-1}. Afforestation followed, with mean marginal costs of \$2,690–2,870 t^{-1} yr^{-1}. Riparian retirement was substantially more expensive despite its higher effectiveness per hectare, with marginal costs ranging from \$12,460 to \$14,150 t^{-1} yr^{-1}. Considerable within-type variation is evident, particularly for riparian retirement (e.g. under M1 the 5^{th}–95^{th} percentile range spans \$7,000 to \$23,610 t^{-1} yr^{-1}). Although riparian retirement produced the largest sediment reductions per hectare, its higher implementation costs, including fencing and planting requirements, resulted in substantially higher marginal costs than afforestation or space-planted trees.
- At an 8% discount rate (Panel C), marginal costs decreased because future costs were more heavily discounted. Space-planted trees declined to \$720–730 t^{-1} yr^{-1}, afforestation to \$1,620–1,720 t^{-1} yr^{-1}, and riparian retirement to \$7,480–8,490 t^{-1} yr^{-1}. Although absolute costs decreased, the relative ranking of mitigation types remains unchanged. This occurs because discounting affects all mitigations in a similar manner and therefore does not substantially alter their relative cost-effectiveness.

Panels D and E report the cost-effectiveness of improving visual clarity, expressed as the cost per metre increase in clarity at the SOE site (\$ million m^{-1}). These values were derived by linking predicted sediment load reductions to clarity improvements using the established nonlinear sediment–clarity relationship. Consequently, the relative ranking of mitigation measures for improving visual clarity closely reflects their ranking for reducing suspended sediment loads.

- At a 2% discount rate (Panel D), space-planted trees provided the lowest cost per unit of clarity improvement, averaging \$7.2–7.4 million m^{-1}. Afforestation produced slightly higher costs of \$16.0–16.6 million m^{-1}. Riparian retirement was substantially more expensive, with costs ranging from \$69.2 – \$87.4 million m^{-1}, reflecting higher implementation costs relative to clarity improvements.
- At an 8% discount rate (Panel E), costs declined proportionally: space-planted trees decrease to \$4.3–4.4 million m^{-1}, afforestation to \$9.6–10.0 million m^{-1}, and riparian retirement to \$41.6–52.5 million m^{-1}. As with sediment reduction, discounting reduced absolute costs but does not change the relative ranking of mitigation options.

Table 15. Distribution of mitigation effectiveness and cost-effectiveness for future mitigation scenarios M1–M3, assuming mitigations were implemented during 2024–2045. Panels show (A) effectiveness of works ($t\ yr^{-1}\ ha^{-1}$), (B–C) marginal cost of sediment load reduction ($\$\ t^{-1}\ yr^{-1}$) at 2% and 8% discount rates, and (D–E) marginal cost of improving visual clarity ($\$$ million m^{-1}) at 2% and 8% discount rates

	Scenario	Mitigation type	Mean	STD	CV	P05	Q1	Median	Q3	P95
(A) Effectiveness of mitigations ($t\ yr^{-1}\ ha^{-1}$)	M1	Afforestation	4.9	2.0	0.41	2.3	3.1	4.8	6.0	8.8
		Riparian retirement	6.1	3.6	0.59	3.4	3.8	5.1	7.8	11.2
		Space-planted trees	3.8	1.6	0.41	1.7	2.7	3.7	4.7	6.5
	M2	Afforestation	4.8	2.0	0.41	2.2	3.1	4.7	5.8	8.0
		Riparian retirement	7.5	4.6	0.61	3.5	4.2	5.8	8.5	17.6
		Space-planted trees	3.8	1.5	0.41	1.7	2.6	3.6	4.6	6.4
	M3	Afforestation	4.6	1.9	0.41	2.1	3.1	4.5	5.7	7.8
		Riparian retirement	7.5	4.6	0.61	3.5	4.2	5.8	8.5	17.6
(B) Marginal cost of reducing sediment load ($\$\ t^{-1}\ yr^{-1}$), 2% discount rate	M1	Afforestation	2,690	1,240	0.46	1,340	1,910	2,370	3,540	5,080
		Riparian retirement	14,150	5,970	0.42	7,000	9,010	13,670	18,160	23,610
		Space-planted trees	1,190	530	0.45	600	830	1,050	1,460	2,240
	M2	Afforestation	2,770	1,240	0.45	1,430	1,930	2,410	3,540	5,360
		Riparian retirement	12,460	6,240	0.50	4,080	8,280	13,100	16,700	20,590
		Space-planted trees	1,210	540	0.45	600	840	1,090	1,490	2,260
	M3	Afforestation	2,870	1,290	0.45	1,450	2,000	2,490	3,550	5,410
		Riparian retirement	12,470	6,240	0.50	4,080	8,280	13,100	16,700	20,590
(C) Marginal cost of reducing sediment load ($\$\ t^{-1}\ yr^{-1}$), 8% discount rate	M1	Afforestation	1,620	750	0.46	800	1,150	1,420	2,130	3,050
		Riparian retirement	8,490	3,580	0.42	4,200	5,410	8,210	10,910	14,180
		Space-planted trees	720	320	0.45	360	500	630	870	1,350
	M2	Afforestation	1,660	750	0.45	860	1,160	1,450	2,130	3,220
		Riparian retirement	7,480	3,750	0.50	2,450	4,970	7,870	10,030	12,360
		Space-planted trees	730	330	0.45	360	500	650	890	1,360
	M3	Afforestation	1,720	780	0.45	870	1,200	1,490	2,130	3,250
		Riparian retirement	7,490	3,750	0.50	2,450	4,970	7,870	10,030	12,360

	Scenario	Mitigation type	Mean	STD	CV	P05	Q1	Median	Q3	P95
(D) Marginal costs of improving water clarity ($ million m^{-1}), 2% discount rate	M1	Afforestation	16.6	7.7	0.46	8.3	11.8	14.7	21.9	31.4
		Riparian retirement	87.4	36.9	0.42	43.2	55.7	84.5	112.3	146.0
		Space-planted trees	7.4	3.3	0.45	3.7	5.1	6.5	9.0	13.9
	M2	Afforestation	16.4	7.4	0.45	8.5	11.4	14.3	21.0	31.6
		Riparian retirement	73.8	37.0	0.50	24.2	49.0	77.6	98.9	121.9
		Space-planted trees	7.2	3.2	0.45	3.6	5.0	6.4	8.8	13.4
	M3	Afforestation	16.0	7.2	0.45	8.1	11.1	13.8	19.7	30.1
		Riparian retirement	69.2	34.7	0.50	22.6	46.0	72.7	92.7	114.3
(E) Marginal costs of improving water clarity ($ million m^{-1}), 8% discount rate	M1	Afforestation	10.0	4.6	0.46	5.0	7.1	8.8	13.2	18.9
		Riparian retirement	52.5	22.2	0.42	26.0	33.5	50.7	67.4	87.6
		Space-planted trees	4.4	2.0	0.45	2.2	3.1	3.9	5.4	8.3
	M2	Afforestation	9.6	4.4	0.45	5.1	6.9	8.6	12.6	19.1
		Riparian retirement	44.3	22.2	0.50	14.5	29.4	46.6	59.4	73.2
		Space-planted trees	4.3	1.9	0.45	2.1	3.0	3.9	5.3	8.0
	M3	Afforestation	9.6	4.3	0.45	4.8	6.7	8.3	11.8	18.1
		Riparian retirement	41.6	20.8	0.50	13.6	27.6	43.7	55.7	68.6

Notes: STD is the standard deviation, CV is the coefficient of variation, P05 and P95 are the 5th and 95th percentiles, and Q1 and Q3 are the 1st and 3rd quartiles. All statistics calculated across subwatersheds where each mitigation occurs within each scenario, using weights based on the areas of mitigation. All values are NZ$. Scenario M3 does not include space-planted trees.

4.4 Model evaluation and limitations

4.4.1 SedNetNZ model evaluation

SedNetNZ is designed to predict spatial patterns in erosion and suspended sediment load on a mean annual basis for periods spanning several decades. Evaluating model performance is difficult over such time scales other than comparison with measurements of suspended sediment loads, which has been the main form of SedNetNZ model evaluation (Basher et al. 2018).

In the upper Waitomo catchment, suspended sediment concentration (SSC) and discharge (Q) have been monitored for several decades at the Aranui Caves Bridge site near the catchment outlet, providing a long-term data set suitable for comparison with SedNetNZ predictions. Mean annual suspended sediment loads have been estimated from these data using SSC–Q rating curve methods, with a 36-year monitoring record available (Table 16).

Table 16. Comparison of published suspended sediment concentration–discharge (SSC–Q) rating curve estimates of mean annual suspended sediment load from the 'Waitomo at Aranui Caves Br' site versus LiDAR-based SedNetNZ model predictions

River monitoring site name	SSC–Q rating curve estimates				SedNetNZ modelled mean annual net sediment load estimates (kt yr^{-1})	
	Source	Flow measurement period (year)	Sediment sampling period (year)	SSC–Q sediment loads[a] (kt yr^{-1})	Regionwide non-LiDAR SedNetNZ (Vale & Smith, 2024)	LiDAR-based SedNetNZ (present report)
Waitomo at Aranui Caves Br (1253) Area: 30.8 km^2	Kotze (2007)	86 - 07	90 - 06	5.4	5.8	5.4
	Hicks (2011)	80 - 96	91 - 97	6.9		
	Hoyle (2012)	86 - 11	90 - 10	5.9		
	Hoyle (2014)	86 - 13	90 - 13	5.9		
	WRC gauge data[b]	86 - 22	90 - 20	6.1		

[a] SSC–Q rating curve estimates incorporate TSS-SSC corrections to refine sediment load estimates.

[b] SSC-Q rating curve estimates directly from WRC sediment data analysis gauging software.

While caution is required when comparing SSC–Q rating curve estimates with model predictions across different timescales and periods, our results showed general agreement between modelled loads and observed estimates (Table 16). However, this comparison is indicative only, as it was based on a single site and subject to the inherent limitations of rating curve methods (Asselman 2000; Vercruysse et al. 2017).

Suspended sediment and flow data in the upper Waitomo catchment extend back to 1990. Over this period, land cover and erosion control mitigations (e.g. tree planting and riparian fencing) have probably changed relative to the contemporary baseline represented in the model. This may have resulted in lower modelled loads compared with historical monitoring estimates. However, rating curve estimates derived from multi-decadal records tend to average variability over time, which is important when comparing them with SedNetNZ load predictions.

Comparison with previous modelling

The LiDAR-based SedNetNZ load estimate at the river monitoring site was broadly consistent with previous region-wide modelling (Vale & Smith 2024), although slightly lower (Table 16). These differences partly reflect changes in the representation and extent of soil conservation measures, such as riparian fencing, as well as differences in how erosion processes are represented within the LiDAR DEM–based sub-models.

Evaluating modelled erosion process contributions is challenging because long-term monitoring data cannot be readily partitioned into individual erosion processes. Nevertheless, the LiDAR-based modelling indicated some shifts in the relative contribution of erosion processes compared with the previous region-wide assessment. In general, the relative contribution of shallow landslides decreased, while surface and riverbank erosion increased slightly (Table 17). These shifts in proportional contribution do not necessarily correspond to large changes in absolute sediment loads.

Table 17 shows that shallow landslides remained the dominant sediment source in the Waitomo catchment. Their contribution decreases from 72% in the previous modelling (Table 17) to 61% in the LiDAR-based assessment, although the absolute loads were similar (4.1 vs 4.9 kt yr^{-1}), Surface erosion increased from 25% to 36% of total load, with estimated loads increasing from 1.7 to 2.4 kt yr^{-1}. Riverbank erosion also increased slightly in proportional contribution (3% to 4%), largely reflecting the improved representation and increased length of the DSN derived from LiDAR terrain data (Table 2). This resulted in an approximate 1.5-fold increase in riverbank-erosion load estimates, from 0.17 to 0.26 kt yr^{-1} (Table 17).

Table 17. Comparison of erosion process loads between the LiDAR-based SedNetNZ and the previous region-wide non-LiDAR SedNetNZ results for the upper Waitomo catchment. Total erosion load delivered to the upper Waitomo stream network from each process is shown first as kt yr^{-1}, and then as percentage of the total erosion (%)

	Total erosion load delivered to the stream network from each process					
	LiDAR-based SedNetNZ (present report)			Previous regionwide non-LiDAR SedNetNZ (Vale & Smith 2024)		
Catchment	Shallow landslide erosion	Surface erosion	Riverbank erosion	Shallow landslide erosion	Surface erosion	Riverbank erosion
Upper Waitomo	4.1 61%	2.4 36%	0.26 4%	4.9 72%	1.7 25%	0.17 3%

Overall, the LiDAR-based SedNetNZ modelling provided a more refined representation of erosion processes. Higher-resolution terrain data improved the representation of topographic controls on erosion, while updated sub-models incorporated expanded data sets for calibration. These improvements better captured spatial variability within catchments, which is difficult to represent using lower-resolution terrain data in region-wide modelling.

At the subwatershed scale, erosion processes show greater variability, particularly in lowland areas where riverbank erosion can be locally important. The LiDAR-based approach better represented these finer-scale variations, improving the ability to distinguish between erosion processes that may be underestimated or overgeneralised in region-wide assessments. This improved spatial resolution strengthened the model’s ability to represent contemporary sediment budgets and supported its application for targeting erosion mitigation.

4.4.2 Model limitations

In Section 4.4.2 we outline some specific limitations in terms of each modelling component below. Model outputs should be interpreted in the context of these limitations.

Limited empirical data remains a key challenge for modelling erosion processes across New Zealand's diverse erosion terrains. As a result, model parameterisation must combine available data with expert judgement when representing erosion processes and mitigation effectiveness. Although the LiDAR-based SedNetNZ model improves the representation of erosion processes, some limitations remain due to data constraints and inherent modelling assumptions.

Erosion process representation

In this project, we updated the surface erosion component of the LiDAR-based model to better represent slope length and steepness, improving the representation of topographic controls on convergent upslope contributing areas, following Smith, Herzig et al. (2019). However, key limitations remain in the calculation of the C and K factors in RUSLE, and the availability of high-resolution input data. Improved soils data sets for the Waikato region, such as S-map, may enhance surface erosion estimates in future.

A stocking density–adjusted K factor was introduced in the surface erosion sub-model (Vale et al. 2025a,b) to account for the effects of livestock treading and grazing on erosion. This approach requires several parameters, including grazing intensity, stock type, soil moisture, clay content, soil susceptibility, and grazing history and duration (Donovan & Monaghan 2021). Many of these parameters vary both annually and over longer timescales as farming practices change. However, due to the absence of suitable spatial or long-term data sets, we had to make assumptions for application in a multi-decadal sediment budget model. The result of this is that these sub-model does not represent inter-annual variability explicitly.

Donovan & Monaghan (2021) reported good agreement between modelled and measured soil loss at catchment and farm scales, providing confidence in the general sensitivity of the adjustment. Their analysis indicated that soil damage was most sensitive to stock type, grazing intensity, and clay content (see Figure 2 of Donovan & Monaghan [2021]). Stock unit densities derived from AgriBase® data provided by WRC were used to represent stock type and grazing density. Although these data are temporally static, they provide the best available spatial representation at the catchment scale. In contrast, soil moisture, grazing history, and grazing duration were unavailable and were approximated using values from Donovan & Monaghan (2021), although model sensitivity to these parameters was relatively low.

Shallow landslides are triggered by storm events exceeding rainfall thresholds, resulting in large inter-annual variability in landslide occurrence and sediment yield. SedNetNZ does not simulate this variability directly. Instead, storm-triggered landslide contributions are averaged over a multi-decadal period, as described in Section 3.2.1. Landslide depth was approximated to a constant 1 m; however, actual depths can vary significantly. For example, Phillips et al. (2021) reported typical depths of up to 2 m, while Page et al. (1994) observed scar depths ranging from 0.13–3.9 m, with an average of 0.89 m. Betts et al. (2017) reported depths in various materials, including weakly indurated sandstone (0.2–1.6 m; mean 0.69 ± 0.05 m), moderately indurated sandstone (0.3–1.4 m; mean 0.74 ± 0.05 m), and mudstone (0.3–3.0 m; mean 1.01 ± 0.07 m). Although informative, these data are limited, and we currently lack sufficient data to represent this spatial variation in landslide depths adequately within the model.

We improved riverbank erosion modelling by using a larger data set on bank migration rates for model calibration and LiDAR-derived estimates of bank height, which replaced the earlier reliance on a regional discharge-bank height relationship. Accurate representation of riparian woody vegetation remains important for modelling bank erosion. In this study, riparian vegetation was derived directly from LiDAR data at 1 m resolution, replacing the lower-resolution (15 m) EcoSat Woody layer (Dymond & Shepherd 2004). The LCDB v6 is unsuitable for representing narrow riparian vegetation strips due to its 1 ha minimum mapping unit. The bank migration, bank height, and net bank erosion relationships were developed and evaluated using datasets from the Hawke's Bay and Greater Wellington regions (Smith et al. 2024) and have not been specifically calibrated for the upper Waitomo catchment. Consequently, their application assumes these relationships are transferable to the study area, which introduces additional uncertainty into the riverbank erosion estimates. However, these relationships are based on substantially larger datasets and improved model parameterisation compared with previous SedNetNZ implementations, providing the best available basis for estimating riverbank erosion within the LiDAR-based framework.

Erosion mitigation effectiveness

Reductions in sediment load from hillslope erosion processes are determined by changes in land cover associated with each mitigation type within each scenario. Effectiveness represents the capacity of a mitigation to reduce sediment loads once fully established and is specific to each mitigation type. The effectiveness values used in this modelling are based on simplified interpretations of published data and assume that mitigations achieve full effectiveness once fully mature. However, reported effectiveness varies widely in the literature, and actual performance can differ depending on site conditions and implementation. A comprehensive review of erosion mitigation effectiveness is provided by Phillips et al. (2020).

For conversion from pasture to permanent woody vegetation, we assumed a 90% reduction in mass movement erosion. This value is consistent with reductions typically reported in New Zealand studies (Phillips et al. 2020). Published reductions estimates range from 35% to 91%, with most studies reporting reductions of 70% to 90% in landsliding under closed-canopy vegetation (e.g. indigenous forest, mature pine forest, or scrub) relative to pasture (Hicks 1989, 1990, 1991; Pain & Stephens 1990; Phillips et al. 1990; Marden et al. 1991; Bergin et al. 1993, 1995; Marden & Rowan 1993; Fransen & Brownlie 1995; Hancox & Wright 2005; Smith et al. 2023).

For space-planted trees, an effectiveness value of 70% was adopted based on Hawley and Dymond (1988) and supported by subsequent studies. Empirical evidence for space planting is often derived from individual or small groups of trees rather than hillslope-scale assessments. Reported reductions in erosion range widely (2% to 95%) across New Zealand studies (Phillips et al. 2020), reflecting strong dependence on successful establishment and maintenance (Marden & Phillips 2013). When trees are appropriately spaced (e.g. at c. 10 m) and well maintained, reductions in shallow landsliding of 70% to 95% have been reported (Hawley & Dymond 1988; Douglas et al. 2009, 2013; McIvor et al. 2015).

Estimating the effectiveness of riparian fencing and stock exclusion for reducing riverbank erosion is more uncertain due to limited empirical studies, and stream bank erosion remains one of the least well understood erosion processes in New Zealand (Basher 2013). Bank erosion varies with stream order, channel position, and dominant processes, including mass failure, stock trampling, and fluvial entrainment (Hughes 2016). As a result, the effects of riparian management can be highly variable. Furthermore, the model applies riparian mitigation at the stream-segment scale using a mean buffer width and therefore does not explicitly distinguish between treatment on one or both stream banks, or account for variation in effectiveness along individual stream banks. The effectiveness values applied here fall within the 30% to 90% range reported in published and unpublished studies (Owens et al. 1996; Williamson et al. 1996; Line et al. 2000; Meals & Hopkins 2002; McKergow et al. 2003, 2007, 2022; Monaghan & Quinn 2010; Phillips et al. 2020).

Riparian fencing estimate

We estimated riparian fencing in the upper Waitomo catchment using spatial data on riparian retirement and fencing provided by WRC. Although these layers represent the best available information, several limitations arose when mapping them onto the DSN to estimate fencing proportions.

A key challenge was the difference in spatial precision between the riparian layers and the mapped stream network. Riparian polygons represent fenced or retired areas, but their boundaries do not always align with the channel position. As a result, direct intersection between the data sets can miss fencing that is functionally adjacent to streams. To address this, we applied a 10 m buffer to the riparian polygons to improve their intersection with the correct stream segments. This buffer width was selected through testing to balance two issues: narrow buffers may underestimate fencing by missing genuine intersections, while wider buffers risk intersecting neighbouring stream segments and inflating estimated fenced length.

Additional limitations arose from reliance on the WRC spatial data sets. Riparian fencing undertaken independently of WRC programmes might not be represented in their database and therefore would not be captured in the modelling. In some cases, older riparian retirement areas have since matured into woody vegetation and are more appropriately represented as woody cover rather than fenced pasture margins.

Accurate estimation of fencing proportions was also influenced by the precision of the DSN. Stream networks are sensitive to the drainage-area threshold used to initiate first-order streams, meaning some first-order streams in the digital network may be perennial, ephemeral, or absent on the ground. To improve representation, we generated a new DSN from the 5 m LiDAR DEM using a 5 ha initiation threshold. Although some over- and under-estimation of channel extent remained, the updated network provided a substantial improvement over the previous REC2 network in representing stream extent and planform.

Riparian buffers were represented using a mean buffer width for each stream segment and therefore do not explicitly account for variation in buffer width, fencing, or vegetation between individual stream banks or along the length of a stream segment. Consequently, local differences in riparian management, and their influence on sediment trapping and bank protection, are simplified within the catchment-scale modelling framework.

Errors in estimating current riparian fencing will influence the modelled effectiveness of future mitigations. Overestimation of existing fencing will reduce the remaining stream length available for additional fencing, thereby limiting modelled reductions in sediment loads and associated improvements in visual clarity and achievement of NPS-FM 2020 attribute bands. Conversely, underestimation of existing fencing may lead to overestimation of the benefits achievable through future fencing.

Karst landscape and sediment routing

Developing a DSN for a catchment underlain by karst geology introduces uncertainties beyond those encountered in conventional surface-water drainage systems. In karst terrain, surface channels often disappear into sinkholes (tomo), dolines, and other dissolution features, transferring flow underground before re-emerging downstream. This behaviour complicates the representation of hydrological connectivity and creates challenges for accurately modelling sediment routing.

We used a LiDAR-derived DEM to generate the DSN, based on surface topography. However, because the DEM cannot resolve subsurface flow pathways, it may depict continuous surface flow where no channel exists, particularly where streams sink into sinkholes. These artefacts required substantial manual editing to remove or adjust in our models. The true hydrological pathways in karst catchments are often discontinuous, complex, and only partially mapped. As a result, digital flow paths may not function in reality if water is captured by underground conduits, while downstream reconnection points may not appear in the DEM at all. This leads to uncertainty in determining where surface flow is genuinely routed and where it transitions into subterranean flow before resurfacing elsewhere in the catchment.

It can also be difficult to establish whether a surface channel that terminates abruptly reconnects further downstream, links to a neighbouring subwatershed, or is confined to a closed karst depression. These uncertainties directly affect sediment routing in the model. If surface flow is assumed to continue downslope along a DEM-derived pathway, sediment loads may be routed to the wrong sub-catchment. Conversely, if flow is assumed to terminate within a karst feature when it actually resurfaces downstream, sediment delivery may be underestimated.

To reduce these limitations, we incorporated available geological and cave-system mapping and drew on the expert knowledge of members of the New Zealand Speleological Society, who provided insight into known subterranean connections in the catchment. Their input helped refine the likely linkages between subwatersheds and identify where surface drainage deviated from DEM-derived pathways. Despite these improvements, some uncertainty remains unavoidable due to the inherently complex and partially unmapped nature of the subsurface karst system.

Reductions required to meet visual clarity attribute bands

We estimated mean annual suspended sediment load reductions to achieve visual clarity and suspended fine sediment objectives using equations developed by Hicks et al. (2019) from simplifications in the relationships reported by Dymond et al. (2017). A key assumption for calculating required load reductions to meet objectives is that the relationship between suspended sediment load and the flow frequency distribution remain constant at a site. In reality, this relationship may change due to changes in catchment hydrology, leading to changes in the relationship between a given flow and suspended sediment load (Hicks et al. 2019).

Because data are not presently available to predict these changes, we have assumed that the associated relationships remain constant. This assumption was particularly important when modelling changes in visual clarity under different scenarios. Because these scenarios may significantly change the land cover and catchment hydrology, the relationship between visual clarity and sediment load may differ at an SOE site compared with the contemporary baseline (C2024).

We estimated the required load reductions using empirical models fitted to a national data set. This should result in the models being fitted to a wide range of catchment variables and therefore representing the variability found in the upper Waitomo catchment. Although sites from Waikato were used in the national data set (see Hicks et al. 2019), this approach may lead to under- or overestimation of required reductions at any one location.

Cost-effectiveness

A key limitation of our cost-effectiveness analysis is the uncertainty associated with sediment yield estimates, which vary spatially and temporally. Baseline sediment loads and the effectiveness of mitigations depend on factors such as topography, land use, and hydrological processes. Although these factors are incorporated to some extent, modelling assumptions and data limitations introduce inherent uncertainty into the results.

The cost-effectiveness analysis also relies on a regression framework to estimate the average contribution of individual mitigations to reductions in sediment load. This approach was used to decompose the combined effects of the modelled mitigation scenarios and estimate the relative effectiveness of different types of mitigation. However, some mitigations are implemented together and are therefore not fully independent, particularly riparian planting and fencing. Consequently, the resulting effectiveness and cost-effectiveness estimates should be interpreted as average marginal effects derived from the suite of modelled scenarios rather than precise estimates of the independent effect of each type of mitigation. Alternative scenario configurations or mitigation combinations may produce different estimates.

The choice of discount rate is another important consideration. The (New Zealand) Treasury recommends a 2% discount rate for environmental projects and an 8% rate for sensitivity analysis (New Zealand Treasury 2024). Higher discount rates substantially reduce the present value of long-term costs and therefore influence the relative cost-effectiveness of mitigations.

We assumed that mitigations were implemented gradually over the study period; however, in practice they are likely to occur sequentially. A sequential implementation creates opportunities for prioritisation, allowing decision makers to allocate resources based on emerging information, funding availability, and landowner participation. These dynamic decision-making processes were not explicitly represented in our analysis and may influence the realised effectiveness and cost-effectiveness of interventions.

Finally, our analysis focused on direct financial costs and sediment reduction benefits. It did not account for opportunity costs or broader co-benefits such as biodiversity enhancement, water quality improvements, carbon sequestration, or cultural values. These factors could substantially influence the overall value of mitigations for landowners and policymakers considering wider environmental and social outcomes.

5 Conclusions

This report describes the application of the LiDAR-based SedNetNZ model to estimate erosion and suspended sediment loads in the upper Waitomo catchment, extending earlier implementation in four Waikato CEM catchments. The model estimates a contemporary suspended sediment load of 5.7 kt yr^{-1} delivered to the catchment outlet. Shallow landslides are the dominant sediment source, contributing ~61% of the load, followed by surface erosion (~36%) and riverbank erosion (~4%). Under a retrospective scenario where erosion mitigations are removed, the modelled load increases to 8.5 kt yr^{-1}, highlighting the importance of existing erosion control mitigations.

Scenario modelling (M1–M3), shows that mitigations including afforestation/bush retirement, space-planted trees, and riparian fencing could reduce sediment loads by 24–45% across the catchment. However, at the Tumutumu monitoring SOE site a 36% reduction from contemporary loads is required to meet the NPS-FM national bottom line for visual clarity, and none of the mitigation scenarios achieved this threshold, further reductions of 17% (M1), 13% (M2), and 6% (M3) would still be required. This indicates that additional or more extensive mitigation would be required to meet the NPS-FM objective.

The cost-effectiveness analysis shows substantial variation in both overall performance of the mitigation scenarios and the effectiveness of individual mitigation types across the catchment. Among the modelled scenarios, M1 provided the lowest cost per unit reduction in suspended sediment load, while M2 and M3 achieved progressively greater sediment reductions but at increasing overall cost. Space-planted trees provided the most cost-effective option for reducing suspended sediment loads and improving visual clarity, while afforestation offered moderate cost-effectiveness. Riparian retirement achieved the highest sediment reductions per hectare but remained the least cost-effective option due to its higher implementation costs and limited total reductions from this mitigation. Although changes in the discount rate affected absolute marginal costs, they do not alter the relative ranking of mitigation types. These cost-effectiveness estimates should be interpreted as indicative average marginal values derived from the modelled mitigation scenarios rather than precise estimates of the independent effects of individual mitigations. Overall, the results highlight the importance of spatially targeted mitigation to improve the efficiency of erosion control investments.

Modelled sediment loads were broadly consistent with estimates derived from SSC–Q rating curves and previous region-wide modelling, supporting confidence in the overall magnitude of predicted loads. The use of high-resolution LiDAR DEMs improved representation of terrain and erosion processes; however, in this karst-dominated catchment, subsurface drainage through sinkholes and cave systems introduces inherent uncertainty in hydrological connectivity and sediment routing.

6 Acknowledgements

We thank Waikato Regional Council for funding this work and the contribution of Waikato Regional Council staff, particularly Tim Norris and Haydon Jones, for their input in defining the project scope, and Paul Smith for organising a catchment visit. We also thank John Ash, Jonathan Davies, and Dave Meikle from the New Zealand Speleological Society for their time and assistance in understanding the Waitomo cave systems subsurface network. We thank Annette Semadeni-Davies for her thorough peer review and constructive feedback on the report.

7 References

Asselman NEM 2000. Fitting and interpretation of sediment rating curves. Journal of Hydrology 234(3–4): 228–248. https://doi.org/10.1016/S0022-1694(00)00253-5

AssureQuality. (2020). AgriBase®. https://www.asurequality.com/services/other-services/agribase/

Basher L 2013. Erosion processes and their control in New Zealand. In: Dymond J ed. Ecosystem services in New Zealand – conditions and trends 2013. Lincoln, Manaaki Whenua Press. Pp. 363–374.

Basher L, Spiekermann R, Dymond J, Herzig A, Ausseil A-G 2018. SedNetNZ, SLUI and contaminant generation. Part1: Sediment and water clarity. Manaaki Whenua – Landcare Research Contract Report LC3135, prepared for Horizons Regional Council.

Bergin DO, Kimberley MO, Marden M 1993. How soon does regenerating scrub control erosion? New Zealand Forestry 38(2): 38–40.

Bergin DO, Kimberley MO, Marden M 1995. Protective value of regenerating tea-tree stands on erosion-prone hill country, East Coast, North Island, New Zealand. New Zealand Journal of Forestry Science 25: 3–19.

Betts H, Basher L, Dymond J, Herzig A, Marden M, Phillips C 2017. Development of a landslide component for a sediment budget model. Environmental Modelling & Software 92: 28–39.

Betts H, Smith HG, Neverman A, Tsyplenkov A, 2023. Wairoa shallow landslide and debris deposit mapping following storm events in March 2022. Landcare Research Contract Report LC4331 for Hawke's Bay Regional Council.

Betts H, Spiekermann R, Dymond J 2017. SedNetNZ modelling of sediment sources and loads from the Western Waikato, Coromandel, Waihou-Piako and Taupo Water Management Zones, Waikato Region. Manaaki Whenua – Landcare Research Contract Report LC2835, prepared for Waikato Regional Council

Booker D, Hicks M 2013. Estimating wetted width and fish habitat areas across New Zealand's rivers: wetted widths estimation. NIWA client report CHC2013-075, prepared for Department of Conservation. Wellington, NIWA.

Brune GM 1953. Trap efficiency of reservoirs. Eos, Transactions American Geophysical Union 34(3): 407–418.

Carter JV, Pan J, Rai SN, Galandiuk S 2016. ROC-ing along: evaluation and interpretation of receiver operating characteristic curves. Surgery 159: 1638–1645.

Conoscenti C, Rotigliano E, Cama M, Caraballo-Arias N, Lombardo L, Agnesi V 2016. Exploring the effect of absence selection on landslide susceptibility models: a case study in Sicily, Italy. Geomorphology 261: 222–235.

Curran-Cournane FC, McDowell R, Littlejohn R, Condron L 2011. Effects of cattle, sheep, and deer grazing on soil physical quality and losses of phosphorus and suspended sediment losses in surface runoff. Agriculture, Ecosystems & Environment 140: 264–272.

Dairy Environment Leadership Group 2013. Sustainable Dairying: Water Accord: a commitment to New Zealand by the dairy sector. http://www.dairynz.co.nz/what-we-do/dairyindustry-strategy/

De Rose R, Basher LR. 2011. Measurement of river bank and cliff erosion from sequential LiDAR and historical aerial photography. Geomorphology 126:132–147.

Desmet P, Govers G 1996. A GIS procedure for automatically calculating the USLE LS factor on topographically complex landscape units. Journal of Soil and Water Conservation 51(5): 427–433.

Donovan M 2022. Modelling soil loss from surface erosion at high resolution to better understand sources and drivers across land uses and catchments: a national-scale assessment of Aotearoa, New Zealand. Environmental Modelling & Software 147: 105228. https://doi.org/10.1016/j.envsoft.2021.105228.

Donovan M, Monaghan R 2021. Impacts of grazing on ground cover, soil physical properties and soil loss via surface erosion: a novel geospatial modelling approach. Journal of Environmental Management 287: 112206. https://doi.org/10.1016/j.jenvman.2021.112206.

Douglas G, Dymond J, McIvor I 2008. Monitoring and reporting of whole farm plans as a tool for affecting land use change. Report for Horizons Regional Council. Palmerston North, AgResearch.

Douglas GB, McIvor IR, Manderson AK, Koolaard JP, Todd M, Braaksma S 2013. Reducing shallow landslide occurrence in pastoral hill country using wide spaced trees. Land Degradation and Development 24: 103–114.

Douglas GB, McIvor IR, Manderson AK, Todd M, Braaksma S, Gray RAJ 2009. Effectiveness of space-planted trees for controlling soil slippage on pastoral hill country. In: Currie LD, Lindsay CL eds. Nutrient management in a rapidly changing world. Occasional Report No. 22. Palmerston North, Fertilizer and Lime Research Centre, Massey University. Pp. 501–513.

Dymond JR, Ausseil AG, Shepherd JD, Buettner L 2006. Validation of a region-wide model of landslide susceptibility in the Manawatu–Wanganui region of New Zealand. Geomorphology 74: 70–79.

Dymond JR, Betts HD, Schierlitz CS 2010. An erosion model for evaluating regional land-use scenarios. Journal of Environmental Modelling Software 25(3): 289–298.

Dymond JR, Davies-Colley RJ, Hughes AO, Matthaei CD 2017. Predicting improved optical water quality in rivers resulting from soil conservation actions on land. Science of the Total Environment 603: 584-592.

Dymond J, Herzig A, Basher L, Betts HD, Marden M, Phillips CJ, et al. 2016. Development of a New Zealand SedNet model for assessment of catchment-wide soil-conservation works. Geomorphology 257: 85–93.

Dymond JR, Shepherd JD 2004. The spatial distribution of indigenous forest and its composition in the Wellington region, New Zealand, from ETM+ satellite imagery. Remote Sensing of Environment 90: 116–125.

Elliott AH, Semadeni-Davies AF, Shankar U, Zeldis JR, Wheeler DM, Plew DR, et al. 2016. A national-scale GIS-based system for modelling impacts of land use on water quality. Environmental Modelling & Software 86: 131–144.

Eyles GO 1983. The distribution and severity of present soil erosion in New Zealand. New Zealand Geographer 39(1): 12–28.

Foster GR, Meyer LD, Onstad CA 1977. A runoff erosivity factor and variable slope length exponents for soil loss estimates. Transactions of the ASAE 20(4): 683–687.

Fransen PJB, Brownlie RK 1995. Historical slip erosion in catchments under pasture and radiata pine forest, Hawke’s Bay hill country. New Zealand Journal of Forestry 40(4): 29–33.

Fuller IC, Riedler RA, Bell R, Marden M, Glade T 2016. Landslide-driven erosion and slope-channel coupling in steep, forested terrain, Ruahine Ranges, New Zealand, 1946–2011. Catena 142: 252–268.

Gill MA 1979. Sedimentation and useful life of reservoirs. Journal of Hydrology 44(1): 89–95.

Hancox GT, Wright K 2005. Analysis of landsliding caused by the February 2004 rainstorms in the Wanganui–Manawatu hill country, southern North Island, New Zealand. Institute of Geological & Nuclear Sciences [GNS} Science Report 2005/11. Wellington, GNS.

Hawke D 1976. The Waitomo Stream, Waitomo Glow-worm Cave, New Zealand. In: Proceedings of the 11th Conference of the Australasian Speleological Federation, pp. 140–145.

Hawley JG, Dymond JR 1988. How much do trees reduce landsliding? Journal of Soil and Water Conservation 43(6): 495–498.

Hicks DL 1989. Storm damage to bush, pasture and forest: some evidence from Cyclone Bola. DSIR Land Resources Technical Record PN2. Palmerston North, DSIR.

Hicks DL 1990. Landslide damage to pasture, pine plantations, scrub and bush in Taranaki. DSIR Land Resources Technical Record 31. Lower Hutt, DSIR.

Hicks DL 1991. Erosion under pasture, pine plantations, scrub and indigenous forest: a comparison from Cyclone Bola. New Zealand Forestry 36(3): 21–22.

Hicks DM, Haddadchi A, Whitehead A, Shankar U 2019. Sediment load reductions to meet suspended and deposited sediment thresholds. NIWA Client Report 2019100CH, prepared for Ministry for the Environment. Wellington, NIWA.

Hicks DM, Shankar U, McKerchar A, Basher L, Lynn I, Page M, Jessen M 2011. Suspended Sediment Yields from New Zealand Rivers. Journal of Hydrology (New Zealand) 50(1): 81-142.

Hicks DM, Shankar U 2020. Sediment load reduction to meet visual clarity bottom lines. Memo prepared for Ministry for the Environment. 9 p. https://environment.govt.nz/assets/publications/Files/technical-report-6-sediment-load-reductions-to-meet-visual-clarity-bottom-lines.pdf (accessed Nov 2024).

Hoyle J, Hicks DM & Roulston H. 2012. Sampled suspended sediment yields from the Waikato region. Waikato Regional Council Technical Report 2012/01, NIWA Client Report CHC2011-135.

Hoyle J. 2014. Waikato suspended sediment indicators: State and trend. Waikato Regional Council Technical Report 2014/43, NIWA Client Report CHC2014-057. Wellington, NIWA.

Hughes AO 2016. Riparian management and stream bank erosion in New Zealand. New Zealand Journal of Marine and Freshwater Research 50 (2): 277–290.

Kimberley MO 2019. Riparian characteristics of pastoral waterways in the Waitomo catchment in 2019. Report prepared by Environmental Statistics Ltd, November 2019 for Waikato Regional Council.

Klik A, Haas K, Dvorackova A, Fuller IC 2015. Spatial and temporal distribution of rainfall erosivity in New Zealand. Soil Research 53: 815–825.

Kotze C, Grant S, Hill R 2007. Suspended sediment monitoring report 2007. Environment Waikato Technical Report 2008/30. Hamilton, Waikato Regional Council.

Land Information New Zealand (LINZ) 2021. Waikato LiDAR 1m DEM (2021). https://data.linz.govt.nz/layer/113203-waikato-lidar-1m-dem-2021/ (accessed July 2024).

Laurenson S, Houlbrooke DJ, Beukes PC, 2016. Assessing the production and economic benefits from preventing cows grazing on wet soils in New Zealand. Journal of the Science of Food and Agriculture 96: 4584–4593.

Leathwick J, Wilson G, Rutledge D, Wardle P, Morgan F, Johnston K, McLeod M, Kirkpatrick R 2003. Land Environments of New Zealand. Auckland, David Bateman.

Line DE, Harman WA, Jennings GD, Thompson EJ, Osmond DL 2000. Nonpoint-source pollutant load reductions associated with livestock exclusion. Journal of Environmental Quality 29: 1882–1890.

Manderson A, Douglas G, Mackay A, Dymond JR 2011. SLUI Outcomes project: review of the SLUI database and development of a SLUI outcomes reporting framework. Report prepared for Horizons Regional Council by AgResearch.

Marden M 2012. Effectiveness of reforestation in erosion mitigation and implications for future sediment yields, East Coast catchments, New Zealand: a review. New Zealand Geographer 68: 24–35.

Marden M, Phillips CJ 2013. Survival and growth of poplar and willow pole plantings on East Coast hill country. Landcare Research Contract Report LC1622, prepared for Plant and Food Research.

Marden M, Phillips CJ, Rowan D 1991. Declining soil loss with increasing age of plantation forests in the Uawa catchment, East Coast region. In: Henriques PR ed. Proceedings, International Conference on Sustainable Land Management, Napier, Hawke's Bay, New Zealand, 17–23 November 1991. Pp. 358–361.

Marden M, Rowan D 1993. Protective value of vegetation on Tertiary terrain before and during Cyclone Bola, East Coast, North Island, New Zealand. New Zealand Journal of Forestry Science 23: 255–263.

McCool DK, Foster GR, Mutchler CK, Meyer LD 1989. Revised slope length factor for the universal soil loss equation. Transactions of the ASAE 32(5): 1571–1576.

McIvor I, Clarke K, Douglas G 2015. Effectiveness of conservation trees in reducing erosion following a storm event. In: Currie LD, Burkitt LL eds. Proceedings, 28th Annual Fertiliser and Lime Research Centre Workshop 'Moving farm systems to improved attenuation'. Occasional Report 28. Palmerston North, Fertiliser and Lime Research Centre.12 pp. https://flrc.massey.ac.nz/workshops/15/Manuscripts/Paper_McIvor_2_2015.pdf (accessed 10 September 2025).

McIvor I, Douglas G, Dymond JR, Eyles G, Marden M 2011. Pastoral hillslope erosion in New Zealand and the role of poplar and willow trees in its reduction. In: Godone D, Stanchi eds. Soil erosion issues in agriculture. London, IntechOpen Pp. 257–278. http://www.intechopen.com/articles/show/title/pastoral-hill-slope-erosion-in-new-zealand-and-the-role-of-poplar-and-willow-trees-in-its-reduction (accessed 10 September 2025).

McKergow LA, Matheson F, Goeller B 2022. Riparian buffer design guide: design to meet water quality objectives. National Institute of Water and Atmospheric Research (NIWA). Available at: https://niwa.co.nz/files/NIWA%20Riparian%20Guidelines_March%202023.pdf

McKergow LA, Tanner CC, Monaghan RM, Anderson G 2007. Stocktake of diffuse pollution attenuation tools for New Zealand pastoral farming systems. NIWA Client Report HAM2007-161 prepared for Pastoral 21 Research Consortium. Hamilton, NIWA.

McKergow LA, Weaver DM, Prosser IP, Grayson RB, Reed AE 2003. Before and after riparian management: sediment and nutrient exports from a small agricultural catchment, Western Australia. Journal of Hydrology 270(3-4): 253–72.

Meals DW, Hopkins RB 2002. Phosphorus reductions following riparian restoration in two agricultural watersheds in Vermont, USA. Water Science and Technology 45(9): 51–60.

Ministry for the Environment (MfE) 2022. Guidance for implementing the NPS-FM sediment requirements. Wellington, Ministry for the Environment.

Ministry for the Environment (MfE) 2020. National Policy Statement for Freshwater Management 2020. Wellington, Ministry for the Environment.

Monaghan RM, Quinn J 2010. Appendix 9: Farms. National Institute of Water and Atmospheric Research (NIWA), Waikato River Independent Scoping Study. Hamilton, NIWA.

Nearing MA, Yin S, Borrelli P, Polyakov VO 2017. Rainfall erosivity: an historical review. Catena 157: 357–362.

Neverman A, Smith HG, Herzig A, Basher LR 2021. Modelling baseline suspended sediment loads and load reductions required to achieve draft freshwater objectives for Southland. Manaaki

Whenua – Landcare Research Contract Report LC3749, prepared for Environment Southland.

Newsome PFJ, Wilde RH, Willoughby EJ 2008. Land Resource Information System spatial data layers: data dictionary. Palmerston North, Landcare Research. http://digitallibrary.landcareresearch.co.nz/cdm/ref/collection/p20022coll14/id/67.

New Zealand Treasury 2024. Treasury Circular 2024/15: updated public sector discount rates for cost benefit analysis. Wellington, The Treasury. https://www.treasury.govt.nz/publications/circulars/treasury-circular-2024-15-updated-public-sector-discount-rates-cost-benefit-analysis (accessed February 2025).

Owens LB, Edwards WM, Van Keuren RW 1996. Sediment losses from a pastured watershed before and after fencing. Journal of Soil and Water Conservation 51(1): 90–94.

Page MJ, Reid LM, Lynn IH 1999. Sediment production from Cyclone Bola landslides, Waipaoa catchment. Journal of Hydrology (NZ) 38: 289–308.

Page MJ, Trustrum NA, Dymond JR 1994. Sediment budget to assess the geomorphic effect of a cyclonic storm, New Zealand. Geomorphology 9(3): 169–188.

Pain CF, Stephens PR 1990. Storm damage assessment using digitised aerial photographs: Eltham, New Zealand, 24–25 February 1986. New Zealand Geographer 46: 21–25.

Palmer D, Dymond J, Basher L 2013. Assessing erosion in the Waipa catchment using the New Zealand Empirical Erosion Model (NZeem®), Highly Erodible Land (HEL), and SedNetNZ models. Landcare Research Contract Report LC1685, prepared for Waikato Regional Council.

Palmer D, Dymond J, Herzig A, Betts H, Marden M, Basher L 2015. SedNetNZ modelling of the Waikato catchment. Landcare Research Contract Report LC2428, prepared for Waikato Regional Council.

Phillips C, Basher L, Spiekermann R 2020. Biophysical performance of erosion and sediment control techniques in New Zealand: a review. Landcare Research Contract Report LC3761, prepared for the Smarter Targeting of Erosion Control (STEC) MBIE research programme.

Phillips C, Betts, H, Smith HG, Tsyplenkov A 2024. Exploring the post-harvest ‘window of vulnerability’ to landslides in New Zealand steepland plantation forests. Ecological Engineering 206: 10N7300. https://doi.org/10.1016/j.ecoleng.2024.107300

Phillips C, Hales T, Smith H, Basher L 2021. Shallow landslides and vegetation at the catchment scale: a perspective. Ecological Engineering173: 106436. https://doi.org/10.1016/j.ecoleng.2021.106436.

Phillips C, Marden M, Basher LR 2018. Geomorphology and forest management in New Zealand’s erodible steeplands: an overview. Geomorphology 307: 107–121.

Phillips CJ, Marden M, Pearce A 1990. Effectiveness of reforestation in prevention and control of landsliding during large cyclonic storms. In: Proceedings of the 19th World IUFRO Congress (Division 1, Vol. 1), Montreal, Canada, August 1990. Pp. 340–350.

Polyakov M, Walsh P, Daigneault A, Vale S, Phillips C, Smith H 2024. Cost-effectiveness of erosion mitigation to meet water clarity targets in the Manawatū-Whanganui Region of New Zealand. Journal of Environmental Management 359: 120991. https://doi.org/10.1016/j.jenvman.2024.12099

Reichenbach P, Rossi M, Malamud BD, Mihir M, Guzzetti F 2018. A review of statistically-based landslide susceptibility models. Earth-Science Reviews 180: 60–91.

Reid LM, Page MJ 2002. Magnitude and frequency of landsliding in a large New Zealand catchment. Geomorphology 49: 71–88.

Renard KG 1997. Predicting soil erosion by water: a guide to conservation planning with the Revised Universal Soil Loss Equation (RUSLE). Washington, DC, United States Government Printing.

Rosewell CJ, Loch RJ 2002. Estimation of the RUSLE soil erodibility factor. In: McKenzie N, Coughlan K, Cresswell H eds. Soil physical measurement and interpretation for land evaluation. Melbourne, CSIRO Publishing Pp. 337–352.

Semadeni-Davies A, Elliott S 2016. Modelling the effect of stock exclusion on *E. coli* in rivers and streams: national application. MPI Technical Paper No. 2017/10. Wellington, MPI.

Smith HG, Herzig A, Dymond JR, Basher LR 2019. Application of a revised SedNetNZ model to the Oreti and Aparima catchments, Southland. Manaaki Whenua – Landcare Research Contract Report LC3507, prepared for Our Land & Water National Science Challenge.

Smith HG, Neverman A, Betts H, Herzig A 2024. Improving understanding and management of erosion with LiDAR. Landcare Research Contract Report LC4466, prepared for Hawke's Bay Regional Council.

Smith HG, Neverman AJ, Betts H, Spiekermann R 2023. The influence of spatial patterns in rainfall on shallow landslides. Geomorphology 437: 108795. https://doi.org/10.1016/j.geomorph.2023.108795

Smith HG, Spiekermann R, Betts H, Neverman AJ 2020. Application of a revised bank erosion model to update SedNetNZ results for Hawke's Bay. Manaaki Whenua – Landcare Research Contract Report LC3740, prepared for Hawke's Bay Regional Council.

Smith HG, Spiekermann R, Betts H, Neverman AJ 2021. Comparing methods of landslide data acquisition and susceptibility modelling: Examples from New Zealand. Geomorphology 381: 107660. https://doi.org/10.1016/j.geomorph.2021.107660

Smith HG, Spiekermann R, Dymond J, Basher L 2019. Predicting spatial patterns in riverbank erosion for catchment sediment budgets. New Zealand Journal of Marine and Freshwater Research 53(3): 338–362.

Snelder T, Biggs B, Weatherhead M 2010 New Zealand River Environment Classification User Guide. March 2004 (Updated June 2010), ME Number 499. https://environment.govt.nz/assets/publications/acts-regs-and-policy-statements/rec-user-guide-2010.pdf

Spiekermann RI, McColl S, Fuller I, Dymond J, Burkitt L, Smith HG 2021. Quantifying the influence of individual trees on slope stability at landscape scale. Journal of Environmental Management 286: 112194. https://doi.org/10.1016/j.jenvman.2021.112194

Trimble SW 1994. Erosional effects of cattle on streambanks in Tennessee, USA. Earth Surface Processes and Landforms 19(5): 451–464.

Vale S, Smith H 2024. Application of SedNetNZ in the Waikato region to support NPS-FM 2020 implementation. Manaaki Whenua – Landcare Research Contract Report LC4432, prepared for Waikato Regional Council.

Vale SS, Smith HG, Neverman A, Herzig A 2021. Application of SedNetNZ with land management and climate change scenarios and temporal disaggregation in the Bay of Plenty Region. Manaaki Whenua – Landcare Research Contract Report LC4002, prepared for Bay of Plenty Regional Council.

Vale S, Smith H, Polyakov M 2025a. Catchment-scale LiDAR-based SedNetNZ modelling in Waikato CEM catchments. Manaaki Whenua – Landcare Research Contract Report LC4588 for Waikato Regional Council.

Vale S, Smith H, Polyakov M 2025b. Catchment-scale LiDAR-based SedNetNZ modelling of erosion and suspended sediment loads in Waikato CEM catchments. Bioeconomy Science Institute Contract Report 2526-0045 for Waikato Regional Council.

Van Beynen PE, Bialkowska-Jelinska E 2012. Human disturbance of the Waitomo catchment, New Zealand. Journal of environmental management, 108, pp.130–140.

Vercruysse K, Grabowski RC, Rickson RJ 2017. Suspended sediment transport dynamics in rivers: Multi-scale drivers of temporal variation. Earth-Science Reviews 166: 38–52. https://doi.org/10.1016/j.earscirev.2016.12.016

Waikato Regional Council (WRC) 2020. Proposed Waikato Regional Plan Change 1: Waikato and Waipā River Catchments (Decisions Version). Waikato Regional Council Policy Series 2020/02. https://www.waikatoregion.govt.nz/assets/WRC/Volume-2-Proposed-Waikato-Regional-Plan-Change-1-Decisions-version.pdf (accessed September 2024).

Wang G, Gertner G, Liu X, Anderson A 2001. Uncertainty assessment of soil erodibility factor for revised universal soil loss equation. Catena 46(1): 1–14.

Whitehead AL, Booker DJ 2020. NZ river maps: an interactive online tool for mapping predicted freshwater variables across New Zealand. Christchurch, NIWA. https://shiny.niwa.co.nz/nzrivermaps/

Williamson R, Smith C, Cooper A 1996. Watershed riparian management and its benefits to a eutrophic lake. Journal of Water Resources Planning and Management 122: 24–32.

Wischmeier WH, Johnson C, Cross B 1971. Soil erodibility nomograph for farmland and construction sites. Journal of Soil and Water Conservation 26(5): 189–193.

Wischmeier WH, Smith DD 1978. Predicting rainfall erosion losses– a guide to conservation planning, agriculture handbook. Indiana, USA, United States Department of Agriculture.

Woods R, Hendrikx J, Henderson R, Tait A 2006. Estimating mean flow of New Zealand rivers. Journal of Hydrology (New Zealand) 45(2): 95–109.

Yang X, Gray J, Chapman G, Zhu Q, Tulau M, McInnes-Clarke S 2018. Digital mapping of soil erodibility for water erosion in New South Wales, Australia. Soil Research 56(2): 158–170.

Zhang X, Liu X, Zhang M, Dahlgren RA, Eitzel M 2010. A review of vegetated buffers and a meta-analysis of their mitigation efficacy in reducing nonpoint source pollution. Journal of Environmental Quality 39(1): 76–84.

Appendix 1 – Summary of layers delivered

Table A1.1. Summary of layers, and attribute fields, associated with the LiDAR-based version of SedNetNZ supplied with the present report

Folder name	Layer name	Description and attribute fields
Watershed_layers	Waitomo_streamlines_v1.0.shp	Digital streamlines representing the drainage network with a 5-ha upstream area threshold for channel initiation. • CATCHMENT – catchment name • HydroID – unique identifier of each subwatershed • NextDownID – HydroID of the next downstream subwatershed • LengthKM – streamline length in km • StrOrd – Stream order (1 – 8)
Watershed_layers	Waitomo_subwatershed_v1.0.shp	Subwatersheds draining to segments within the digital stream network. • CATCHMENT – catchment name • HydroID – unique identifier of each subwatershed • NextDownID – HydroID of the next downstream subwatershed • AreaKM2 – subwatershed area in km^2

Folder name	Layer name	Description and attribute fields
Modelled_layers	Waitomo_C2024_LiDAR_SedNetNZ_v1.0.shp	LiDAR-based SedNetNZ suspended sediment budget for each subwatershed in the upper Waitomo catchment based on 2023/24 land cover from LCDB v6.0 and existing soil conservation works (C2024). The shapefile contains the following fields: • HydroID – unique identifier of each subwatershed • NextDownID – HydroID of the next downstream subwatershed • AreaKM2 – subwatershed area in km^2 • LandslYld – mean annual suspended sediment yield (t km^{-2} yr^{-1}) from shallow landslides delivered to the stream segment within a subwatershed • SurfaceYld – mean annual suspended sediment yield (t km^{-2} yr^{-1}) from surface erosion delivered to the stream segment within a subwatershed • EarthflYld – mean annual suspended sediment yield (t km^{-2} yr^{-1}) from earthflow erosion delivered to the stream segment within a subwatershed • GullyYld – mean annual suspended sediment yield (t km^{-2} yr^{-1}) from gully erosion delivered to the stream segment within a subwatershed • RivBankYld – mean annual suspended sediment yield (t km^{-2} yr^{-1}) from net riverbank erosion delivered to the stream segment within a subwatershed • TotalSedYld – total mean annual suspended sediment yield (t km^{-2} yr^{-1}) delivered to the stream segment from all erosion processes present within a subwatershed • AccNetLoad – net suspended sediment load that accumulates downstream while accounting for losses of sediment into long-term storage in lakes and on floodplains (t yr^{-1})
Modelled_layers	Waitomo_MitScenarios_SedYld_LiDAR_SedNetNZ_v1.0.shp	LiDAR-based SedNetNZ total mean annual suspended sediment yield (t km^{-2} yr^{-1}) for each subwatershed in the upper Waitomo catchment based on the erosion mitigation scenarios (M1, M2 and M3). The shapefile contains the following fields: • HydroID – unique identifier of each subwatershed • AreaKM2 – subwatershed area in km^2 • XX_XX_XXX – total mean annual suspended sediment yield (t km^{-2} yr^{-1}) delivered to the stream segment from all erosion processes present within a subwatershed for the respective scenario ○ C2024_yld, M1_yld, M2_yld, M3_yld, retro_yld

Folder name	Layer name	Description and attribute fields
Modelled_layers	Waitomo_ MitScenarios_NetLd_LiDAR_SedNetNZ_v1.0.shp	LiDAR-based SedNetNZ mean annual net suspended sediment load (t yr^{-1}) that accumulates downstream for each subwatershed in the upper Waitomo catchment based on the erosion mitigation scenarios (M1, M2 and M3). The shapefile contains the following fields: • HydroID – unique identifier of each subwatershed • AreaKM2 – subwatershed area in km^2 • XX_XX_XXX – mean annual net suspended sediment load that accumulates downstream while accounting for losses of sediment into long-term storage in lakes and on floodplains for each respective scenario (t yr^{-1}) ○ C2024_nld, M1_nld, M2_nld, M3_nld, retro_nld
Shallow_landslide	Waitomo_XXX_ShallowLandslideErosion_v1.0.tif XXX = • C2024, M1, M2, M3	Raster layer (5 m grid) of mean annual suspended sediment yield (t km^{-2} yr^{-1}) from rainfall-induced shallow landslide erosion delivered to the stream network for contemporary baseline (C2024) and full implementation of each erosion mitigation scenario (M1, M2 and M3). For sediment budgeting, the sediment yield from shallow landslide erosion is derived by averaging across all pixels within a subwatershed.
Surface_erosion	Waitomo_XXX_SurfaceErosion_v1.0.tif XXX = • C2024, M1, M2, M3	Raster layer (5 m grid) of mean annual suspended sediment yield (t km^{-2} yr^{-1}) from surface erosion delivered to the stream for contemporary baseline (C2024) and full implementation of each erosion mitigation scenario (M1, M2 and M3). At the pixel scale, very high sediment yields from surface erosion occur when expressed per km^2 in some cases due to the combination of high erosion rates and the small pixel size (1 pixel = 25 m^2). For sediment budgeting, the sediment yield from surficial erosion is derived by averaging across all pixels within a subwatershed. The sediment yields account for sediment trapping by riparian buffers, which is determined for each subwatershed and applied across all pixels within the subwatershed.

Folder name	Layer name	Description and attribute fields
Visual_clarity	SOE_C2024_proportional_reductions_v1.0.shp SOE_MitScenarios_proportional_reductions_v1.0.shp SOE_C2024_sediment_load_reductions_v1.0.shp SOE_MitScenarios_sediment_load_reductions_v1.0.shp	Modelled reductions in suspended sediment loads for contemporary baseline and erosion mitigation scenarios required to achieve each NPSFM (2020) attribute band and NBL for suspended fine sediment. Provided as proportional reductions and load reductions (t yr^{-1}). • Site_name – Name of SOE monitoring site • Site_ID – Site ID of SOE monitoring site • HydroID – unique identifier of each subwatershed • SedClass – Suspended sediment class (1-4) based on REC segments (Hicks & Shankar (2020)) • CLAR – Estimated baseline visual clarity for each SOE site (based on data provided) • base_stat – Estimated base state (based on data provided) • NBL_XX, B_XX, A_XX - Proportional reductions to achieve NPS-FM (2020) for band A, B and NBL (C). Suffixes refer to respective scenarios. ○ C2024, M1, M2, M3